U.S. Department of Commerce
National Oceanic and Atmospheric Administration
National Weather Service
National Centers for Environmental Prediction
5830 University Research Court
College Park, MD 20740-3818

Office Note 509
https://doi.org/10.25923/26ds-q363.

The NOAA-NCEP 40 year Reanalysis with the Next Generation Global Ocean Data Assimilation System (NG-GODAS): 1979 to 2019

Jong Kim[1,2], Yi-Cheng Teng[1**], Shastri Paturi[1], Guillaume Vernieres[5], Travis Sluka[3], Jieshun Zhu[4], Yan Hao[1], Denise Worthen[1], Bin Li[1], Jun Wang[5], Stylianos Flampouris[1**], Xiao Liu[1], Hyun-Chul Lee[1], Daryl Kleist[5], and Vijay Tallapragada[5]

[1]I.M. Systems Group Inc., Rockville, Maryland

[2]Science and Technology Corp., Hampton, Virginia
[*]The affiliation with I.M. Systems Group Inc. when the work was conducted.

[3]Joint Center for Satellite Data Assimilation, Boulder, Colorado

[4]NOAA/NWS/NCEP/CPC, College Park, Maryland

[5]NOAA/NWS/NCEP/EMC, College Park, Maryland

[**]current affiliation is tomorrow.io.

E-mail: Jong.Kim@noaa.gov

Abstract

The National Oceanic and Atmospheric Administration (NOAA) Unified Forecast System (UFS) marine reanalysis is a global sea ice ocean coupled reanalysis product produced by the the UFS Research-to-Operations (R2O) project. Underlying forecast and data assimilation systems are based on the UFS model prototype version-6 and the NG-GODAS release of the Joint Effort for Data assimilation Integration (JEDI) Sea Ice Ocean Coupled Assimilation (SOCA). Covering the 40 year reanalysis time period from 1979 to 2019, the data atmosphere option was applied to the UFS coupled global atmosphere ocean sea ice model components. Assimilated observation data sets include extensive space-based marine observations and conventional direct measurements of in-situ profile data sets. The release of the UFS-marine interim reanalysis product aims to obtain scientific feedback and applications from the broader weather and earth system modeling and analysis communities for the development of the next generation operational numerical weather prediction system at the National Weather Service (NWS). The released file sets are available at https://registry.opendata.aws/noaa-ufs-marinereanalysis, two parts 1) 1979 - 2019 UFS-DATM-MOM6-CICE6 model free runs and 2) 1979-2019 reanalysis cycle outputs. Analyzed sea ice and ocean variables are ocean temperature, salinity, sea surface height, and sea ice concentration. Information of the ocean biogeochemical reanalysis capability (based on the BLINGv2 model developed at the Geophysical Fluid Dynamics Laboratory) is also presented as an additional coupling option for the UFS-MOM6 system. Developed and distributed by the Joint Center for Satellite Data Assimilation (JCSDA), the JEDI-SOCA system is available at https://github.com/jcsda/soca.

1. Introduction

Since the 1980s, the NOAA National Centers for Environmental Prediction (NCEP) has used the 3D variational data assimilation (3DVar) approach to provide the ocean state analysis and monitoring services [Derber and Rosati (1989)]. Subsequent updates resulted in the 2003 Global Ocean Data Assimilation System [Behringer and Xue (2004)] and the ocean analysis component of the Climate Forecast System [Saha et al. (2006)] as well. However, the GODAS operational environment is now considered to be outdated, since its products demonstrate less than the desired accuracy. Specifically, the current system does not support the assimilation of all the ocean observations, resulting in a lower quality ocean analysis compared to similar products and uses an outdated ocean model version without sea ice model coupling.

In an effort to develop a community-based, coupled, comprehensive modeling and data assimilation framework, the National Weather Service (NWS) has launched the UFS project to modernize the development and operationalization process for a broad spectrum of end-to-end forecasting systems development and operationalization process. The rationale of the UFS project is to maximize efficiencies, leverage new technologies, and enhance predictions. The major UFS project components applied as design and implementation principles include:

- Unification of the data assimilation under the JEDI project
- Development of the coupled model for Atmosphere–Ocean–Ice–Waves
- Modernization of the observations processing
- Unification of the forecast workflow
- Validation and verification of the analysis and forecast

Comprising the core of future operational models for global weather, sub-seasonal and seasonal (S2S) forecasting, the new UFS coupled model system is built on the Finite-Volume Cubed-Sphere (FV3) dynamical core for the atmosphere, the Modular Ocean Model (MOM6) for the ocean, the Goddard Chemistry Aerosol Radiation and Transport (GOCART) for aerosols, the Los Alamos Community Ice Code (CICE6) for the sea-ice, the community Noah land surface model with multi-parameterization (Noah MP/LM4) for land, and the NOAA wave model WAVEWATCH III (WW3) for waves. Following the public release of the JEDI-SOCA repository, the NG-GODAS developement effort has been focused on the integration of the marine UFS components into one system and the prototype production for the operational transition over time. The target applications include the climate monitoring of the ocean services and the continuous development of the marine data assimilation to provide marine initial conditions for the future coupled NWS UFS forecasting systems, e.g., S2S experiments.

As the key milestone updates and benchmark test results of the UFS and JEDI projects become available, the development activities of the ocean data assimilation task have been extended from establishing the prototype version of the JEDI-based NG-GODAS system to the interim 40 year reanalysis production run of the UFS sea ice and ocean model components. Underlying forecast and data assimilation production runs are based on the UFS model prototype version-6 and the NG-GODAS release tag of the JEDI SOCA interface. Covering the 40 year reanalysis time period from 1979 to 2019, the data atmosphere option of the UFS coupled global atmosphere ocean sea ice (DATM-MOM6-CICE6) model was applied with two atmospheric forcing data sets: the Climate Forecast System Reanalysis (CFSR) from 1979 to 1999 and Global Ensemble Forecast System (GEFS) from 2000 to 2019. Assimilated observation data sets include extensive space-based marine observations and conventional direct measurements of in-situ profile data sets. Based on an in-house SOCA-science workflow system, the SOCA 3DVar option was used. The climatology of the DRAKKAR forcing set (DFS52) is used to correct the climatological bias issue in the CFSR.

The reanalysis experiment includes two parts: the 1) 1979 - 2019 UFS DATM-MOM6-CICE6 model free run and 2) 1979-2019 3DVar reanalysis cycle output. A scientific evaluation of the NG-GODAS system was conducted for analyzed sea ice and ocean variables: ocean temperature, salinity, sea surface height, and sea ice concentration. The model free run result and analysis outputs were compared with current operational ocean data assimilation systems including the GODAS and CFSR. Validated against the UK MET office EN4 analysis [Good et al. (2013a)] product, considerably improved temperature and salinity analysis outputs were obtained from the NG-GODAS 3DVar experiments.

This document consists of the following sections. In section 2 we provide the model configurations, including the grid and the physical parameterization schemes of the MOM6 and CICE6 models. A numerical stability requirement of the UFS model free run in long time scale is introduced in terms of the CICE6 B-grid of the UFS model system. In section 3 and 4 we describe the surface forcing bias correction and marine observation data source that we applied for the reanalysis experiment. The JEDI SOCA system and reanalysis experiment setup are described in section 5. After introducing the experiment results in section 5, we conclude with the summary (Section 6) to overview the current status and future plans. Developed by the NOAA Geophysical Fluid Dynamics Laboratory (GFDL), the BLINGv2 ocean biogeochemical model [Dunne et al. (2020)] is also adapted in the NG-GODAS reanalysis with satellite ocean color observations assimilated. The preliminary coupled MOM6-BLINGv2 model free run results and its reanalysis outputs are provided in Appendix B.

2. UFS DATM-MOM6-CICE6 configuration

Several key configuration input parameters applied in the UFS model forecast runs of the MOM6 and CICE6 model components are given in Table 1. The MOM6 is the latest generation ocean model produced by the NOAA GFDL and is substantially different from the previous MOM models. The MOM6 uses a new algorithm, the arbitrary Lagrangian-Eulerian (ALE) algorithm, to allow for any type of vertical grid without having to worry about violating CFL conditions. The configuration used here is the SPEAR [Seamless System for Prediction and EArth System Research; Lu et al. (2020)] 1 degree configuration from GFDL. The ocean and sea ice components use a nominal horizontal resolution of 1° with refinement to 1/3° in the meridional direction in the Tropics. The ocean model has 75 layers in the vertical, with layer thickness as fine as 2 m near the surface, and includes 30 layers in the top 100 m. The vertical grid spacing becomes larger with depth, reaching 250 m below 5,000 m. The default vertical coordinate system used in SPEAR is the hybrid z-isopycnal coordinate. However, due to issues with spurious spread that have been found, our current work with MOM6 is being done with z* coordinates.

Table 1. Key configuration parameters applied in the runs of the MOM6 and CICE6 models.

Parameters	Configurations
Horizontal resolution	Global 1-deg with tropical refinement to about 0.3-deg
Total number of grid points	360x320
Model coupling frequency DT	900 sec
Atmospheric forcing	6 hourly,U/V/T/q/MSLP/DSW/DLW/Precip
MOM6 vertical resolution	75 z* layers with top layer thickness 2m
MOM6 baroclinic time step DT	1800 sec
MOM6 tracer advection time step DT	3600 sec
MOM6 Sea surface salinity relaxation	Monthly WOA climatology;166mm/day
MOM6 River runoff	Dai and Trenberth monthly climatology
Sea ice categories	5

The MOM6 sub-grid-scale physics parameterizations incorporate various features including the small-scale mixing of breaking internal tides, the surface mixed layer, and the mesoscale eddies; see the detailed description in the paper by Adcroft et al. (2019). The following code block shows the portions of the MOM_input namelist file for the parameter options used in the experiment.

```
! ===module MOM_MEKE===
! USE_MEKE = True
! If true, use the MEKE scheme: a sub-grid mesoscale eddy
! kinetic energy budget .
! === module MOM_lateral_mixing_coeffs ===
USE_VARIABLE_MIXING = True
! If true, the variable mixing code will be called.
! === module MOM_set_visc ===
CHANNEL_DRAG = True
! If true, the bottom drag is exerted directly on each
! layer
! === module MOM_mixed_layer_restrat ===
```

```
MIXEDLAYER_RESTRAT = True
! If true, a density-gradient dependent re-stratifying
! flow is imposed in the mixed layer
! === module MOM_diabatic_driver ===
ENERGETICS_SFC_PBL = True
! If true, use an implied energetics planetary boundary
! layer scheme to determine the diffusivity and viscosity
! in the surface boundary layer.
! === module MOM_tidal_mixing ===
INT_TIDE_DISSIPATION = True
! If true, use internal tidal dissipation scheme to drive
! diapycnal mixing, along the lines of St. Laurentetal.
! (2002) and Simmons et al. (2004).
! === module MOM_kappa_shear ===
USE_JACKSON_PARAM = True
! Jackson-Hallberg-Legg (JPO 2008) shear mixing
! parameterization.
! === module MOM_tracer_advect ===
TRACER_ADVECTION_SCHEME = "PPM:H3"
! PPM:H3 - Piecewise Parabolic Method (Huyhn 3rd order)
```

CICE version 6.0.0 [Hunke et al. (2020)] was released in March 2018 with new features including new icepack version 1.1.0 enhanced rheology options, dynamic array allocation, and a simplified initialization procedure, etc. The UFS sea ice model was transitioned to CICE6 in August 2020. Three thermodynamics options are available in the current version, the zero-layer thermodynamics, the Bitz and Lipscomb model Bitz and Ipscomb (1999) that assumes a fixed salinity profile, and a new mushy formulation in which salinity evolves [Feltham et al. (2006)]. The mushy thermodynamics option treats the sea ice as a mushy layer in which the ice is assumed to be composed of microscopic brine inclusions surrounded by a matrix of pure water ice. Both enthalpy and salinity are treated as prognostic variables. We observed that the mushy thermodynamics option provides a stable computational result for the sea ice thermodynamics computation. The ice_in namelist code block for the thermodynamic and dynamic options used in the experiment is given below.

```
&thermo_nml
 kitd                   = 0
 ktherm                 = 2
 conduct                = 'bubbly'
a_rapid_mode            =  0.5e-3
&dynamics_nml
 kdyn                   = 1
 ndte                   = 120
 revised_evp            = .false.
```

3. Surface forcing

The surface forcing for NG-GODAS uses a bulk formulation based on Large and Yeager (2004). With this bulk formulation the fluxes are calculated from the SST of the MOM6 model and the surface fields of the offline atmosphere. Since the model's SST is considered in the calculations, there exists a negative feedback that prevents the model SST from drifting too far away from nature. For this reason, relaxation to an SST product (e.g. OISST, OSTIA) is no longer needed and can be removed entirely if the model/forcing biases are small enough. Since there is no similar negative feedback for ocean salinity, an SSS restoration term is still required.

The NG-GODAS is forced with a set of atmospheric fluxes from CFSR (1989-2000) and GEFS (2000-2019). However, there exist very large known biases in the CFSR fluxes. For instance, in the western tropical pacific and Indian ocean, the downward shortwave radiation from CFSR is too high compared to other reanalysis products that have been calibrated to fit observations. We used the bias correction scheme developed by Sluka (2018) to correct the climatology of the CFSR with the DRAKKAR forcing set [DFS52; Dussin et al. (2016)] for the 1989 to 2000 time period. In the scheme, multiplicative and additive correction factors are calculated for each month of the CFSR-based experiment time period for precipitation rate, downward shortwave, and downward longwave, and wind fields. Applying these corrections to the free-run NG-GODAS, yields modeled SST with less bias (see Figure 1).

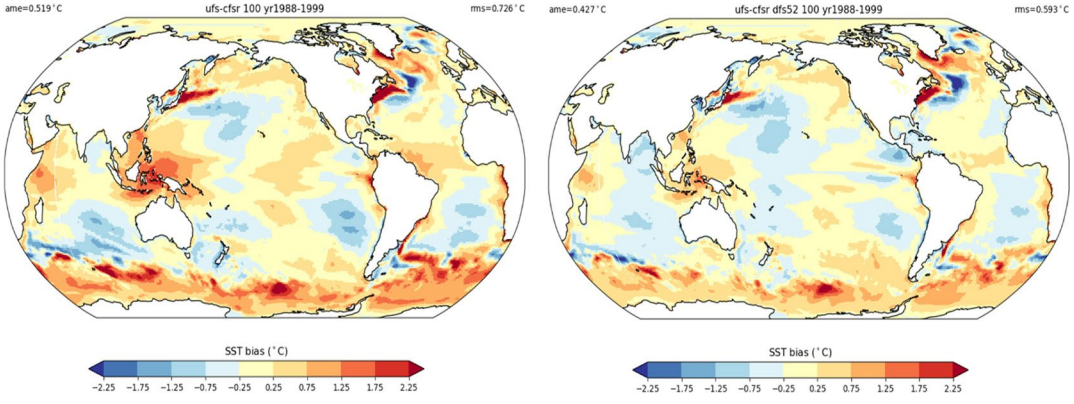

Fig. 1. Difference in the ocean SST from free-run NG-GODAS compared with OISST, averaged over 1989- 2000. Shown is a forced run using uncorrected CFSR fluxes (left) and CFSR fluxes with climatology corrected by DFS5.2 (right).

Figure 2 shows the annual mean wind stress compression between GEFS and CFSR in 2000. The spatial patterns and magnitudes of wind stress calculated by the bulk formulation were comparable between GEFS and CFSR after the forcing bias correction. We further checked the northward global ocean heat transport from simulations with and without bias correction. In Figure 3 , after applying the climatological correction, the CFSR run (red line) exhibits similar northward global ocean heat transport compared to the runs using other forcing (CORE-II and GEFS) along latitude lines.

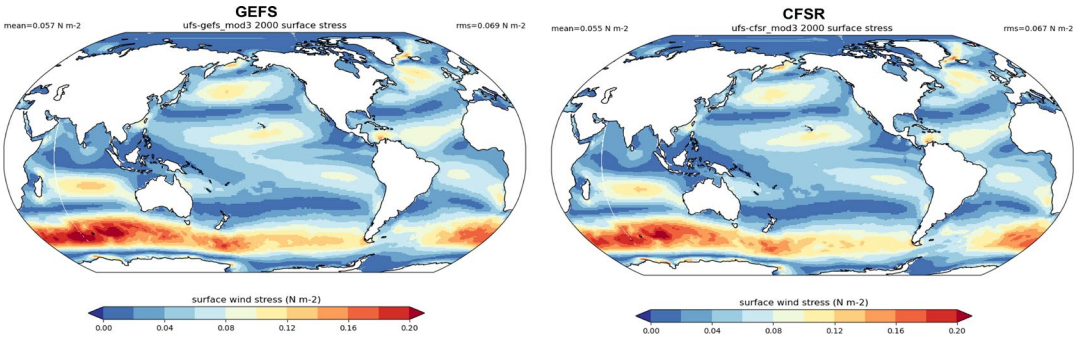

Fig. 2. The 2000 annual mean wind stress calculated from bulk formulation: GEFS (lef) and CFSR after bias correction (right).

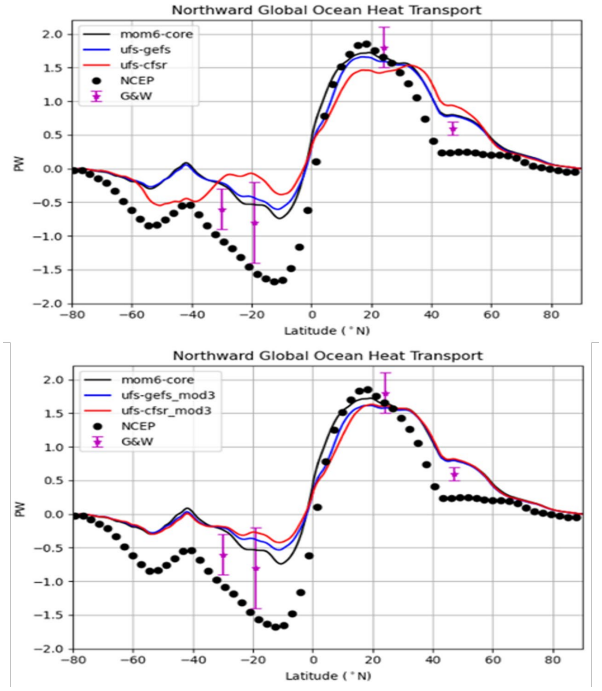

Fig. 3. The 2000 mean northward global ocean heat transport from CORE-II, GEFS, and CFSR simulations (top: no bias correction; bottom: bias correction). Also shown are the implied mean northward global ocean heat transport derived from air-sea surface heat fluxes using NCEP reanalysis data (NCEP) and the observation-based in situ estimates (G&W, Ganachaud and Wunsch (2003)). CORE = Coordinated Ocean-sea ice Reference Experiments.

4. Marine observations

The marine observations in NCEP operational systems consist of in-situ temperature and salinity, sea-ice concentration, satellite sea surface temperature (SST), sea surface salinity (SSS) and absolute dynamic topography (ADT). Diverse data conversion and pre-processing steps are applied to meet the requirements for observation files and I/O handling involved in different modeling and data assimilation systems. Creating a common software system for organizing and storing the vast amounts of observation data is highly desirable to maintain current and future operational forecast systems in a sustainable way. The JEDI-based Interface for Observation Data Access (IODA, https://github.com/JCSDA/ioda) was applied to establish a 40-year historical database of marine observations. By using a common netCDF data format, the IODA data processing allows a practical approach for the creation of historical databases and the long-term storage of data. Figure 4 shows the temporal coverage of the marine observations and data sources that we used in

the NG-GODAS reanalysis experiment. Figures 5 provides a decomposition of the total observation counts by data type applied in the experiment.

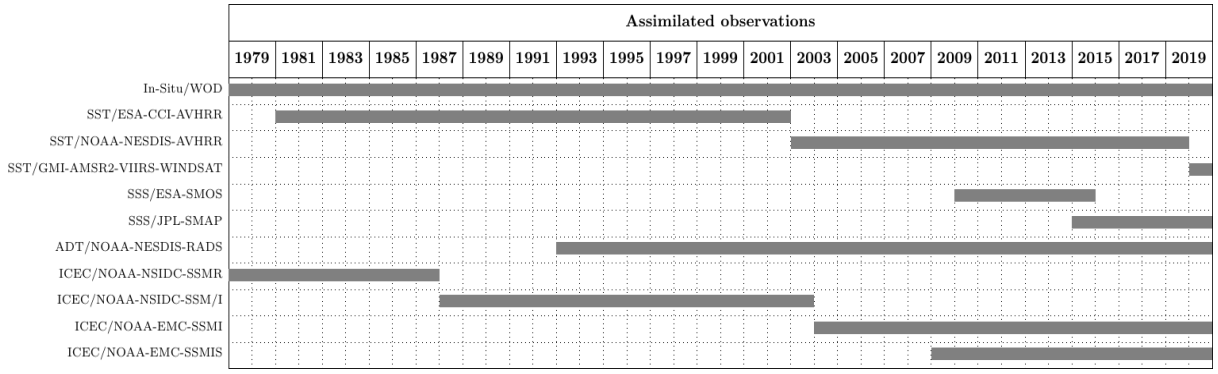

Fig. 4. Temporal coverage of observations assimilated in the reanalysis experiment: remote sensing retrievals and in-situ profile data from 1979 to 2019.

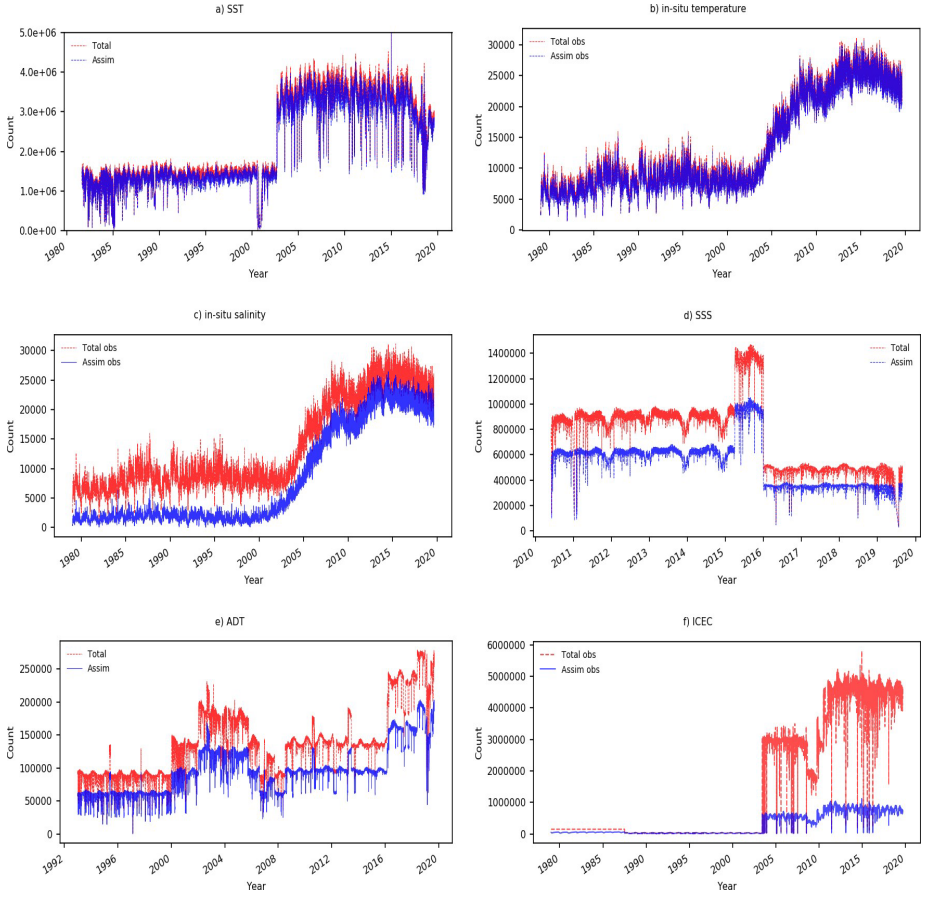

Fig. 5. Total number of observations (total injected observations in red and assimilated ones in blue) applied in each 24 hour analysis cycle window: a) SST, b) in-situ temperature, c) in-situ salinity, d) SSS, e) ADT, and f) ICEC. The total number of observations injected in the assimilation experiment cycles is marked in red and assimilated ones in blue. Quality control schemes applied in the assimilation experiments are described in the Section 5.

We started the reanalysis cycles with the injection of the in-situ water temperature and salinity profile data sets obtained from the World Ocean Database [Boyer et al. (2018)]. In-situ observations provide direct measurements relevant to water temperature and salinity. Since the

spatial resolution of the in-situ marine measurements is not extensive, satellite observations are used to provide uniform coverage in resolving dynamical ocean features. The European Space Agency SST Climate Change Initiative [ESA-CCI SST; Merchant et al. (2019)] data sets are assimulated from 1981 onward to constrain the ocean surface conditions. For the calibrated and quality controlled water temperature at the depth of 0.2 m, the ESA-CCI SST retrievals are based on the Advanced Very High Resolution Radiometer [AVHRR; Embury et al. (2019b)] and Along Track Scanning Radiometer [ATSR; Embury et al. (2019a)] observations. Since 2002, the AVHRR Global Area Coverage (GAC; 4 km) SST retrievals of the NOAA reanalysis version 1 (RAN1) were assimilated in our experiment. Produced with AVHRR data from the five NOAA and two Metop satellites, the RAN1 SST data sets have been matched up with the reference SSTs and the quality controlled in situ SSTs: from the NOAA in situ Quality Monitor (iQuam; https://www.star.nesdis.noaa.gov/sod/sst/iquam) and the Canadian Meteorological Centre GHRSST Level 4 CMC0.2deg Global Foundation Sea Surface Temperature Analysis product (https://www.ncei.noaa.gov/archive/accession/GHRSST-CMC0. 2deg-CMC-L4-GLOB).

The bias-corrected SSTs with the sensor-specific error statistics (SSES) were processed in the JEDI-based IODA data conversion process for the AVHRR RAN1 SST data sets. Satellite SSS measurements are a relatively recent technique. We used the passive microwave L-band radiometry satellite SSS products from the ESA Soil Moisture and Ocean Salin- ity (SMOS; https://earth.esa.int/eogateway/missions/smos/data) and the NASA Aquarius and Soil Moisture Active Passive (SMAP; https://podaac.jpl.nasa.gov/SMAP) missions. The SSS assimilation covers about 7 years in our experiment, starting with the SMOS data from 2011 and the SMAP data from 2015. The ADT observation is the mea- surement of height variations in the surface of the sea with respect to the geoid. The NOAA Radar Altimeter Database System [RADS, Scharroo et al. (2013)] ADT data set from ftp://ftp.star.nesdis.noaa.gov/pub/sod/lsa/rads/adtx includes the dynamic topography measurement of the sea surface height derived by nine altimeter missions: TOPEX/Poseidon, Jason-1, Jason-2, Geosat, GFO, ERS-1, ERS-2, Envisat, and CryoSat-2.

The assimilation of the ADT data set was conducted from 1992 to 2019. Although satellite radar and laser altimeters allow us to monitor sea ice freeboard thickness, obtaining robust sea ice thickness from satellites is still difficult. However, sea-ice concentration remote sensing data sets driven by passive microwave satellites have been more widely used since the start of the satellite era in 1979. We used the NOAA NSIDC [Cavalieri et al. (1996)] and EMC sea ice concentration databases built on the data sets from the Scanning Multichannel Microwave Radiometer (SMMR) instrument on the Nimbus-7 satellite and the Special Sensor Microwave/Imager (SSM/I) and Special Sensor Microwave Imager/Sounder (SSMIS) and instruments on the Defense Meteorological Satellite Program's (DMSP) -F8, -F11,-F13, -F15, -F16, -F17, and -F18 satellites. Figure 6a shows the data count comparison of satellite observations assimilated in the reanalysis experiment. The dominant observation types are satel- lite SST retrievals. From 1981, 1 to 2 million SST data sets are constantly assimilated in each 24 hour analysis window. When the NOAA RAN1 product became available in 2002, the volume of the assimilated SST data further increased. Sea ice concentration observations are consistently assimilated in the experiment as well. Temporal resolution of the NSIDC data set alternately covers every other day from 1979 to 1987 and then daily from 1987. With the EMC-processed SSM/I and SSMIS L2 data sets, about a million sea ice observations were assimilated since 2002. Relatively smaller volumes of the SSS and ADT data sets are assimilated: SSS with about a million observations since 2015 and ADT with about 0.1 million observations since 1993. In-situ observations provide direct measurements relevant to both water temperature and salinity based on sources such as ships, moored and drifting buoys, etc. Figure 6b shows the in-

situ temperature data counts binned according to depth. Since 2002, the Argo deployment contributes to considerably improved spatiotemporal coverage of the in-situ profile data sets.

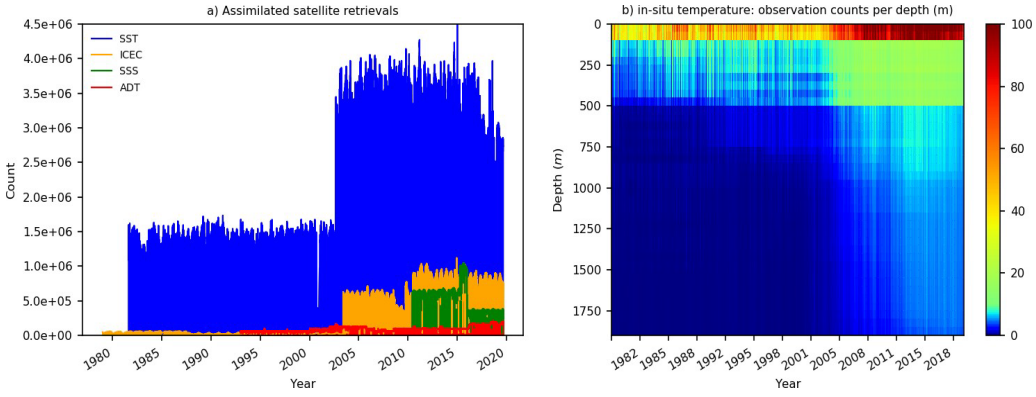

Fig. 6. Observation counts assimilated in each 24 hour analysis cycle window: a) assimilated remote sensing retrievals and b) in-situ temperature data counts binned according to depth.

5. JEDI-SOCA and experiment setup

In the JEDI software structure, the object oriented prediction system (OOPS) provides a core framework of algorithms that combines generic building blocks for data assimilation application algorithms. The programming approach of the OOPS system, mostly written by C++, does not require knowledge of actual implementations of specific application model structures or observation data information. In the JEDI interface-based programming method, application calls are made with a list of the pre-defined OOPS abstract interfaces, rather than by direct calls to any unitary application routines or classes. A few articles [Trémolet (2020); Holdaway et al. (2020); Honeyager et al. (2020)] introduce a key concept of the JEDI software system, to highlight how different data assimilation systems can be seamlessly established through the common software components.

As a core JEDI application project, the SOCA data assimilation system links the OOPS interface classes of Geometry, State, Increment, Model, VariableChange, and LinearVariableChange with the MOM6 and CICE6 models. A C++ traits technique is applied to connect the SOCA application interfaces to the OOPS abstract interfaces and generic algorithms. In addition to the model interfaces, generic marine observation operators and data handling capabilities of the JEDI unified observation (forward) operator (UFO) and interface for observation data access (IODA) systems are also utilized in the SOCA project. The JEDI UFO contains generic quality control options and filters that can be applied to each observation system without coding at certain model application levels. User-specified yaml configuration files are only required in the JEDI UFO applications. Table 2 shows various observation filters applied in the experiment: bounds check, background check, domain check, etc. Observation localization and error inflation schemes were also combined in the filtering processes. Additional Blacklist filters were applied in the experiment to filter out the ADT data set in the south Pacific and western Australia areas.

Table 2. JEDI UFO observation quality control filters applied in the reanalysis experiment.

Observations	Localization: Gaspari-Cohn	Inflate Error	Bound Check	Background Check	Domain Check

SST	200km	factor: 5.0 lat>60,lat<-60	min: -2 max: 36	threshold: 5.0	
SSS	200km		min: 0.1 max: 40.0	threshold: 5.0	SST < 10
In-situ temperature	500km		min: -2 max: 36	threshold: 5.0	T obs error < 0.001
In-situ salinity	500km		min: 1.0 max: 40.0	threshold: 5.0	S obs error < 0.0001
Ice fraction	200km		min: 0 max: 1	threshold: 5.0	SST > 0.9
ADT	500km	factor: 5.0 lat>60,lat<-60	min: -2 max: 2 assign error [0.5,1.0]	|threshold|: 0.2	SST < 5.0

The MOM6-CICE6 coupled data assimilation capabilities of the SOCA have been tested with various JEDI OOPS data assimilation algorithms including 3DVar, 3DEnVar, and 3D-FGAT and their hybrid variants. The NG-GODAS reanalysis experiment is based on the 3DVar option. The estimate of the background error covariance matrix (B) is key to the efficiency and accuracy of the 3DVar algorithm. The JEDI system provides the System Agnostic Background Error Representation (SABER) bundle to build the background error covariance matrix. In the SOCA 3DVar application, the construction of the covariance matrix B is decomposed into several linear operators: a horizontal correlation operator with the BUMP (Background error on an Unstructured Mesh Package; https://github.com/benjaminmenetrier/bump) library, variable transforms of multivariate balance operators, parameterizations of vertical convolution and background errors, and a horizontal noise control filter. Balance operators for the control variables of temperature, salinity and sea surface height follow the cross-correlation schemes implemented by Cooper and Haines (1996), Troccoli et al. (2002), and Weaver et al. (2006). Temperature background error variance is given as a function of vertical temperature gradient and further modulated by pre- computed horizontally varying surface conditions. The SOCA 3DVar yaml input file used for the experiment is provided in Appendix A. The MOM6-CICE6 models are initialized at 12:00 UTC in the 24 hour analysis window cycles and integrated for 24 hour model forecast. For the model free run and 3DVar cycle experiment, the CFSR and GEFS Data atmospheric fluxes are given at 6 hour interval. The MOM6 initial condition was prepared from the 1/4 degree OM4 files and regridded into 1 degree resolution.

Although the sea ice thickness data assimilation option is provided in the current version of the SOCA system, we only applied sea ice concentration observation data sets in the reanalysis experiment. Thus, maintaining the numerical stability of sea ice thickness calculation is a critical step in the reanalysis cycles. We stabilized the sea ice thickness with the climatological sea ice thickness using the data sets of the Global Ice-Ocean Modeling and Assimilation System [GIOMAS; Zhang and Rothrock (2003)] at each analysis checkpoint step. The GIOMAS data set includes monthly ice thickness, concentration, growth/melt rate as well as ocean heat flux from 1970 to present. Figure 7 shows the GIOMAS sea ice thickness distributions applied in the experiment.

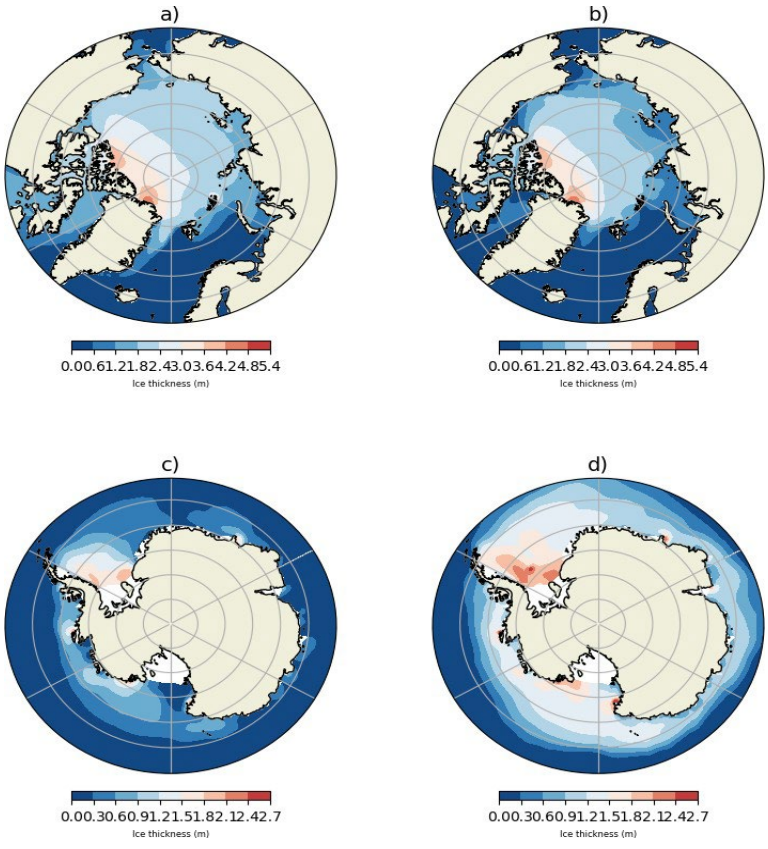

Fig. 7. Seasonal mean sea ice thickness distributions obtained from GIOMAS data for the 1979-2019 time period: a) Arctic DJF (December-January-February), b) Arctic JJA (Jun-July-August), c) Antarctic DJF, and d) Antarctic JJA.

6. Results

To allow public access of the NG-GODAS reanalysis experiment results, the experiment output files were released through the NOAA Big Data Program (BDP): https://registry.opendata.aws/noaa-ufs-marinereanalysis. The AWS opendata registry contains the model free runs and 3DVar analysis outputs: daily MOM6-CICE6 diagnostic output files from 1979-01-01 to 2019-08-30 for both the model states and observations analyzed in the reanalysis experiment. The following diagram shows the directory structure of the released experiment results.

ng−godas −1 deg :

3dvar
- ana
- ana_config
- bkg
- incr
- obs_out
- rst

noda
- bkg
- obs_out
- rst

ChangeLog

- bkg: analysis and model free run background state files with MOM6/CICE6 diagnostic outputs
- ana: analysis model state files
- incr: Obs increment files
- rst: MOM6/CICE6 model restart files with annual frequency
- ana_config: JEDI analysis input config files applied to 3DVAR reanalysis experiment
- 3dvar: analysis cycle outputs

– noda: UFS DATM–MOM6–CICE6 model free run outputs

The quality of the reanalysis results are first demonstrated by the observation-model differences of each experiment set. Model free run and reanalyzed model fields are also validated in comparison with current operational systems and the UK Met Office EN4 ocean analysis product.

Model free run and 3DVar reanalysis statistics

The differences between observations and model background (innovation or OmB) and those between observations and analysis (OmA) are produced in the IODA files. As diagnostic method to quantify the model background and analysis errors in observation space, the OmB and OmA statistics provides information on the statistical quality of the analysis experiment and the contribution of observations. Global mean time-series plots of the OmB and OmA statistics for each observation type are shown in Figures 8 and 9: the error statics are discussed below per observation type. Along with the OmB and OmA statistics for the analysis experiment, the observation fits to the model free run are reported as well. In this case, the forward observation operators are passively applied to the model free run results. Observation errors are needed in the variational data assimilation algorithm to determine the weights of the observation and model background contributions. Figure 10 shows the observation error statistics of each observation type applied the experiment. Although observation data qualities are dependent on observation types and vary along with the reanalysis cycles, consistent assimilation convergence is properly maintained. No signs of over-fitting to observations or unrealistic artifact in model states are found in the global OmB and OmA statistics results as well.

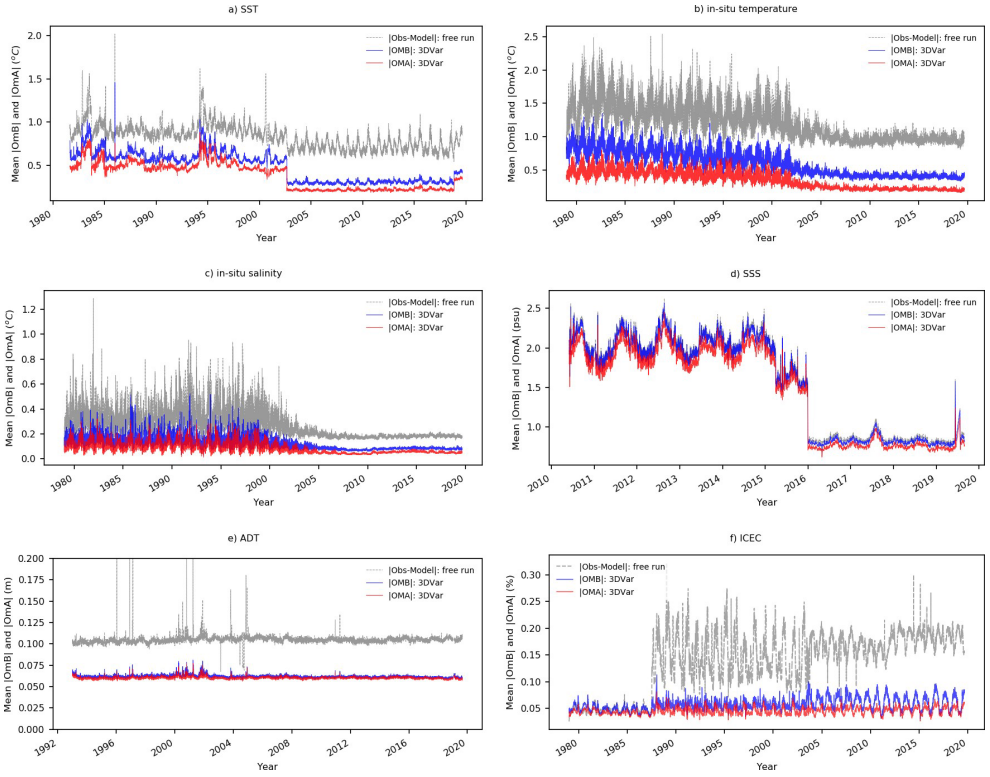

Fig. 8. Global mean absolute errors of observation fits to model free run, model background, and analysis: a) SST, b) in-situ temperature, c) in-situ salinity, d) SSS, e) ADT, and f) ICEC.

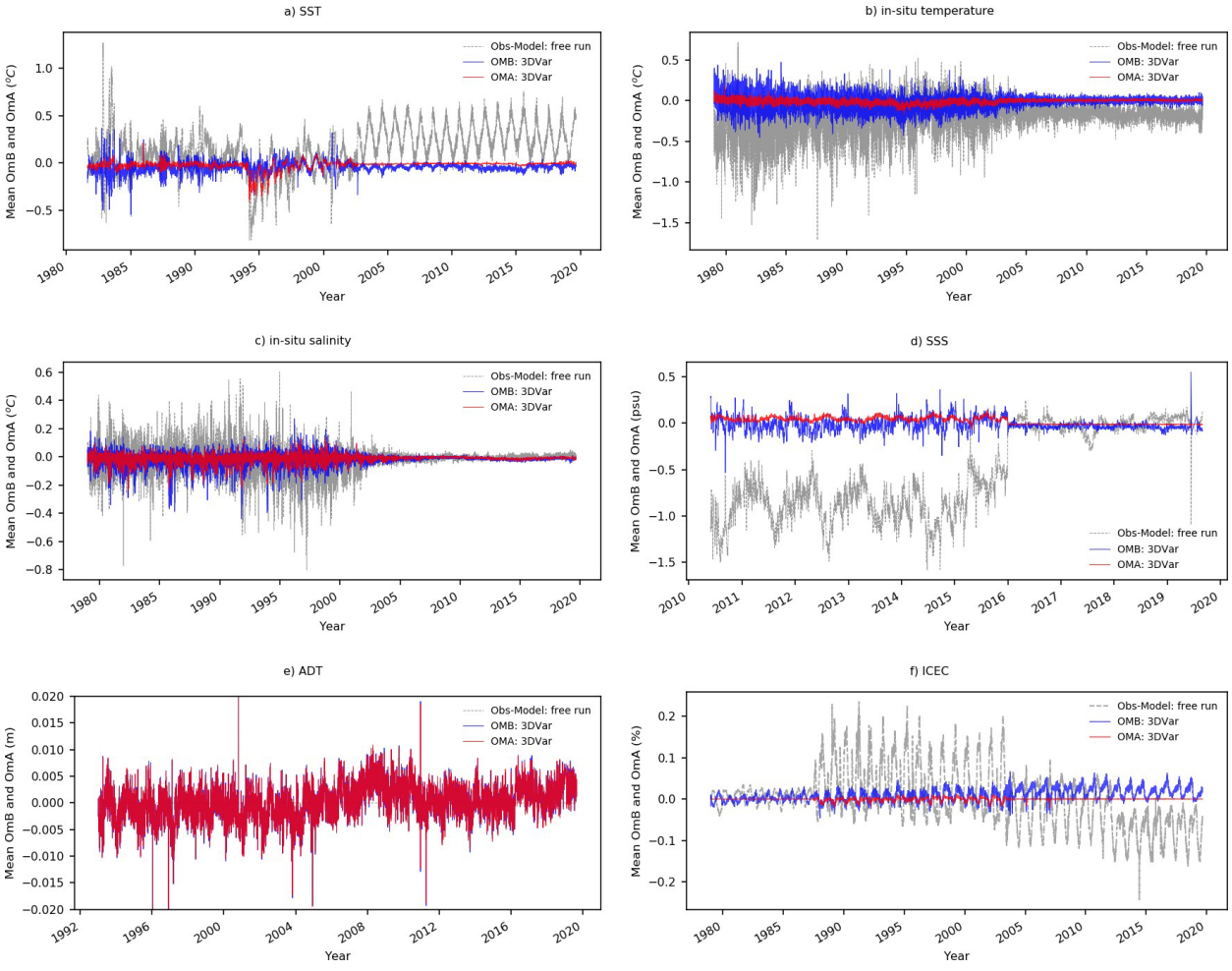

Fig. 9. Global mean errors of observation fits to model free run, model background, and analysis: a) SST, b) in-situ temperature, c) in-situ salinity, d) SSS, e) ADT, and f) ICEC.

Several SST retrievals are assimilated in the experiment: ESA CCI AVHRR (1981-2000), NOAA RAN1 AVHRR (2000-2018), and GHRSST microwave and VIIRS (2018-2019) SST products. The assimilated SST data count increases after 2002 with the assimilation of the METOPA RAN1 SST retrieval data sets: see Figure 6a. The SST analysis statistics are mainly characterized by the observation errors of the SST data set and the fit to the model background states. The large sample size of the RAN1 SST data set results into the reduced OmB and OmA errors. The performance of the SST retrieval processing algorithms are evaluated in the paper by Pryamitsyn et al. (2020): the Advanced Clear-Sky Processor for Oceans (ACSPO) for the RAN1 SST data set and the model-based Optimal Estimation (OE) method for the ESA CCI SST product. The SST bias and standard deviation are validated with the in-situ measurements. The ACSPO-processed SSTs generally account for more clear-sky observations and are more accurate than the ESA CCI SST product. Atmospheric forcing options also contribute to the UFS model SST biases. Depicted in Figure 9a, the SST global mean error statistics shows that the SST cold bias behavior of the model free run tends to be amplified with the GEFS forcing. The latitudinal binning of the SST OmB statistics of the model free run is shown in Figure 11a. A dominant feature is a cold bias over the most of the experiment time period although a seasonally varying warm bias is observed at high latitude areas.

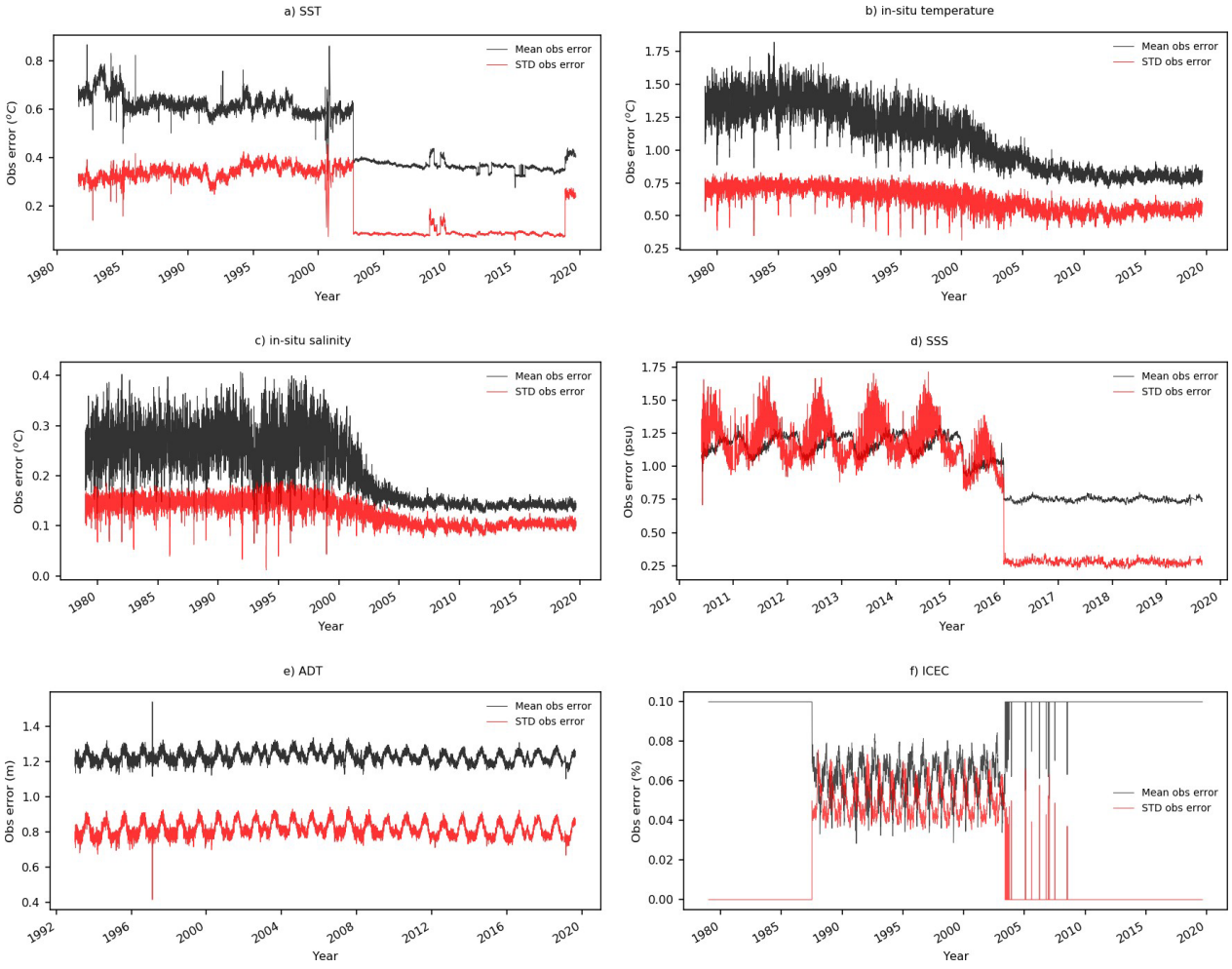

Fig. 10. Global mean errors and standard deviations of each observation type: a) SST, b) in-situ temperature, c) in-situ salinity, d) SSS, e) ADT, and f) ICEC.

The WOD in-situ ocean profile data sets were used to contain the sub-surface ocean condition. Figure 8b and 8c show that the sub-layer temperature and salinity analysis statistics improves with the assimilation of the ARGO float data. After 2004, the in-situ observation sample size increases considerably and data quality improves with the ARGO data set: Figure 6b and 6c. Figure 8b and 8c show that the strong seasonal variability of the OmB and OmA statistics identified during the pre-Argo time period largely disappears when the Argo data are assimilated. Figure 11b shows the vertical binning of the in-situ water temperature statistics of the model free run. As with the SST result, the main features are a model cold bias near the surface layers up to 100 m and a warm bias at sub-surface layers.

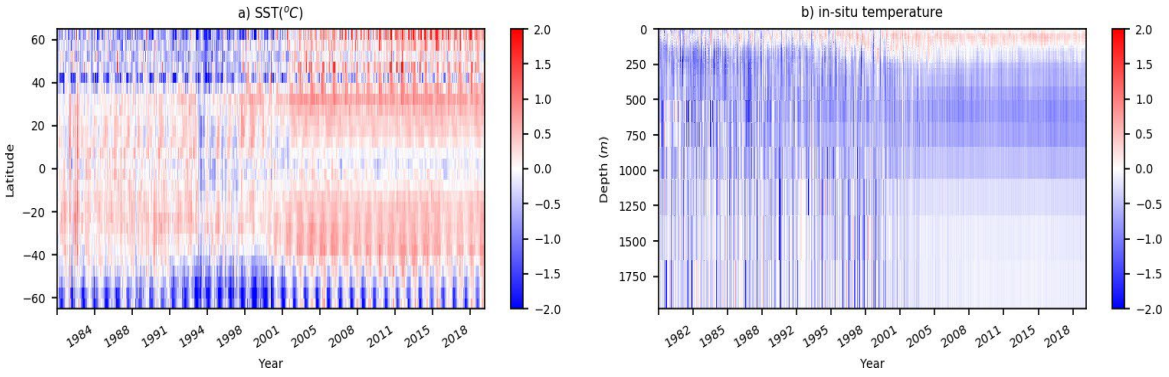

Fig. 11. Global mean absolute errors of observation fits to model free run: a) SST (binning applied according to latitude) and b) in-situ temperature (binning applied according to depth).

The SSS assimilation was conducted with the ESA L2 SMOS data set from 2010 and SMAP SSS from 2015. The observation instrument types and retrieval algorithms significantly affect the SSS retrieval data qualities: antenna type, sampling time, strong land-sea emissivity contrast issue, etc. Figure 8d shows that the SMAP data provides improved SSS assimilation results. In the figure, the SSS statistics are cross-compared with the in-situ salinity assimilation result as well. Seasonally-varying systematic errors and negative bias in the model free run are noticeable featuresin the SMOS SSS statistics. But such problems are largely contained with the SMAP and Argo salinity data sets. The shift around 2015 and 2016 is the main contributor to the better SMAP SSS data quality.

Figure 8e shows that ADT observations from the Radar Altimeter Data System (RADS) are in good agreement with the model results. Relatively small fluctuations are identified but all within modest scales. These changes most likely occur with satellite data reductions and transitions in the 1990s and early 2000s when the ERS-2 and Jason-1 data sets are assimilated. Several sea ice data sources are used in the experiment: the SSMR From 1979 to 1987, SSMI from 1988 to 2004, and the EMC-processed SSMI and SSMIS from 2004 to 2019. Constant observation error application to the SSMR and EMC-processed SSMI and SSMIS data sets results in an increased uncertainty level in marginal ice concentration areas. Figure 8f shows that the global mean of the absolute errors of the OmB and OmA statistics increase during the Arctic melting season. Thus, seasonal variation in the observation fits to model results is a common feature in the experiment.

Diagnostic validation

To evaluate the performance of NG-GODAS, its monthly mean temperature and salinity are further validated against the UK Met Office Hadley Centre EN4.0.2 [hereafter referred to as EN4; Good et al. (2013b)]. The EN4 is an objective monthly analysis based on in situ ocean observations and has 42 levels ranging from 5 to 5350 meters in depth on a global 1° x 1° grid from 1990 to present. Our evaluation period is 2001-2019, since we consider the EN4 to be more reliable after the advent of Argo than before. Also, since a different atmospheric forcing (i.e., bias corrected CFSR) is prescribed for the NG-GODAS reanalysis before 2000, the evaluations for 2001-2019 will be less impacted by the forcing adjustment. NG-GODAS performance is compared to two NOAA ocean analyses – GODAS [Behringer and Xue (2004)] and CFSR [Saha et al. (2010)], which are used in many operations at NOAA (e.g., GODAS is used as a monitoring tool for global ocean status, ENSO diagnostic discussions, MJO status and so on; CFSR is used to initialize the CFSv2, the current NOAA subseasonal and seasonal prediction system).

Figure 12 demonstrates the mean difference in the upper ocean temperature and salinity relative

to the EN4. For temperature, GODAS (Figure 12a) and CFSR (Figure 12b) have a generally comparable bias amplitude over most regions, even though CFSR presents a larger warm bias in the equatorial and far eastern Pacific and a large cold bias in the tropical north Atlantic. The temperature bias in NG-GODAS (Figure 12c) is smaller than GODAS and CFSR over the Gulf Stream region, the equatorial Indian and Pacific regions and the Antarctic Circumpolar Current (ACC) region. One exception is the equatorial Atlantic when NG-GODAS has a slightly larger temperature bias than GODAS. For salinity, there are large biases over the global ocean in GODAS (Figure 12d) and CFSR (Figure 12e), such as the freshening bias over the entire tropical ocean, and the CFSR has even a larger bias. The large salinity bias in mean states is somewhat unexpected for the GODAS and CFSR, because even though they do not assimilate real salinity profiles, they do assimilate synthetic salinity profiles that are generated using temperature profiles and climatological T-S relationships. The procedure is supposed to make the model salinity climatology close to the observed. For salinity in NG-GODAS (Figure 12f), the mean bias is clearly smaller than that for GODAS and CFSR over all global ocean. Over the equatorial Atlantic, however, NG-GODAS presents a clear salinity bias as for temperature. For the middle-depth ocean (Figure 13), the temperature mean bias pattern for the three reanalyses is generally similar to their upper ocean counterparts (Figure 12), and NG-GODAS (CFSR) demonstrates the smallest (largest) biases. The mean salinity biases at mid-depth are different from those at the upper ocean, with salty biases appearing in most oceans. Among the three reanalysis products, CFSR demonstrates the largest salinity difference from the EN4 and NG-GODAS presents the highest consistency.

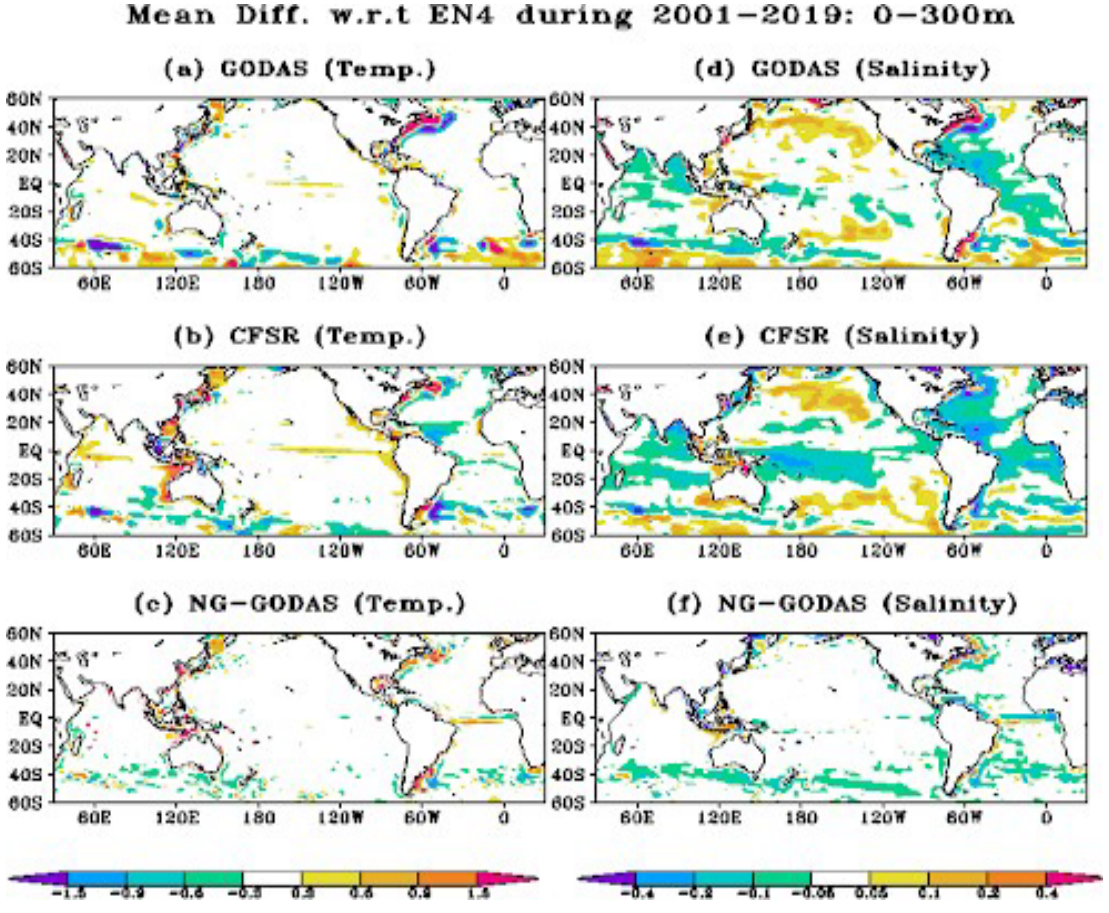

Fig. 12. Mean difference of (a-c) temperature (unit: °C) and (d-f) salinity (unit: psu) vertically averaged over 0-

300m during 2001-2019 with respect to the EN4 analysis in (a, d) GODAS, (b, e) CFSR, and (c, f) NG-GODAS.

To highlight the performance of NG-GODAS in the tropical Pacific, Figure 14 and Figure 15 show the vertical structures of the temperature and salinity biases along the equator and a meridional section (115°W) in the eastern Pacific, respectively. Along the equator (Figure 14), both GODAS and CFSR present the large and warm biases together with freshening biases along the thermocline depth. In comparison, CFSR demonstrates larger biases, with temperature (salinity) biases reaching 1.5°C (-0.3psu). The biases are significantly improved in NG-GODAS, with temperature (salinity) biases mostly smaller than 0.5°C (0.1psu). The superiority of NG-GODAS over GODAS and CFSR is also evident in the meridional-vertical sections of temperature and salinity biases (Figure 15).

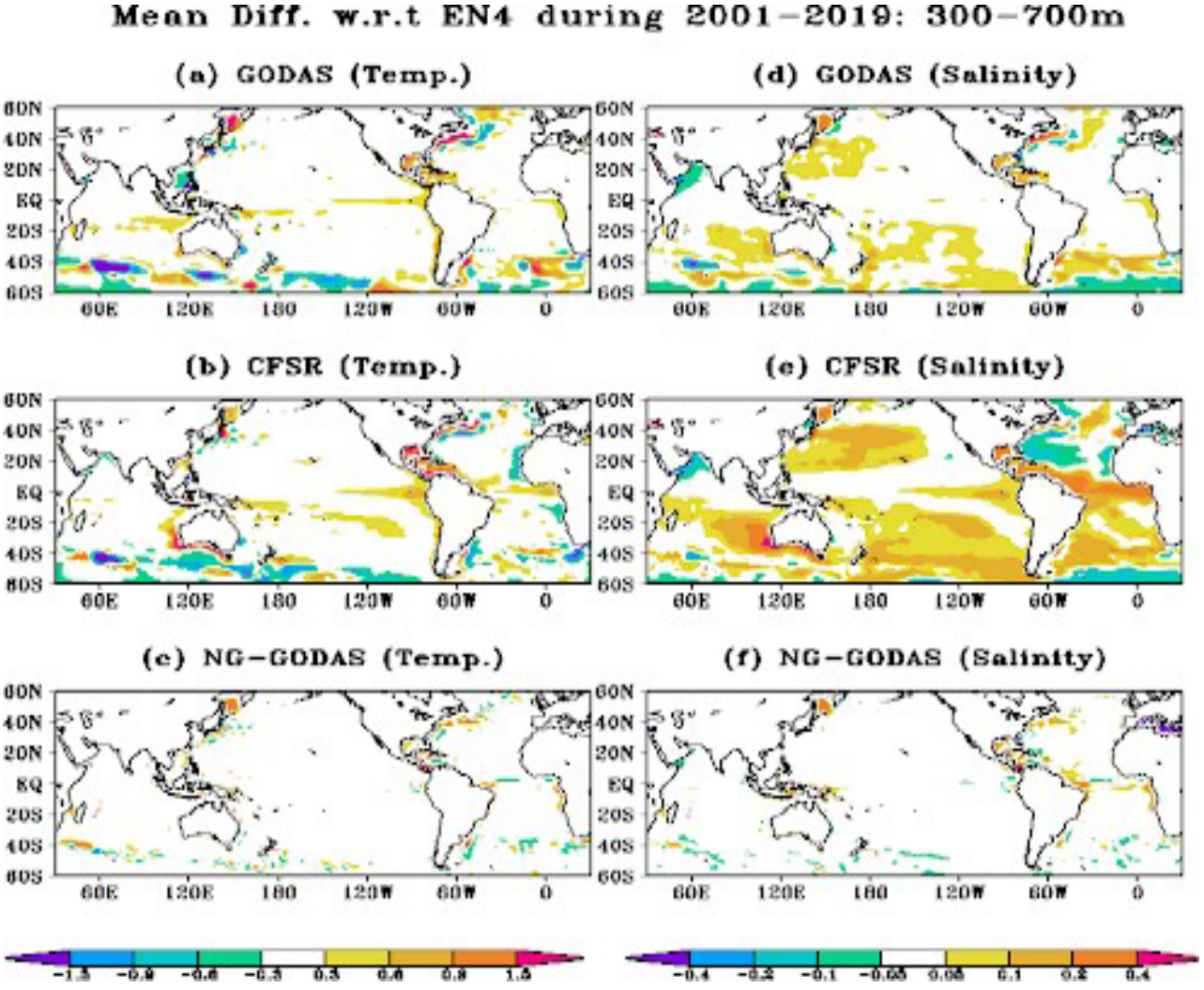

Fig. 13. As in Fig. 12, but for (a-c) temperature (unit: °C) and (d-f) salinity (unit: psu) averaged over 300-700m.

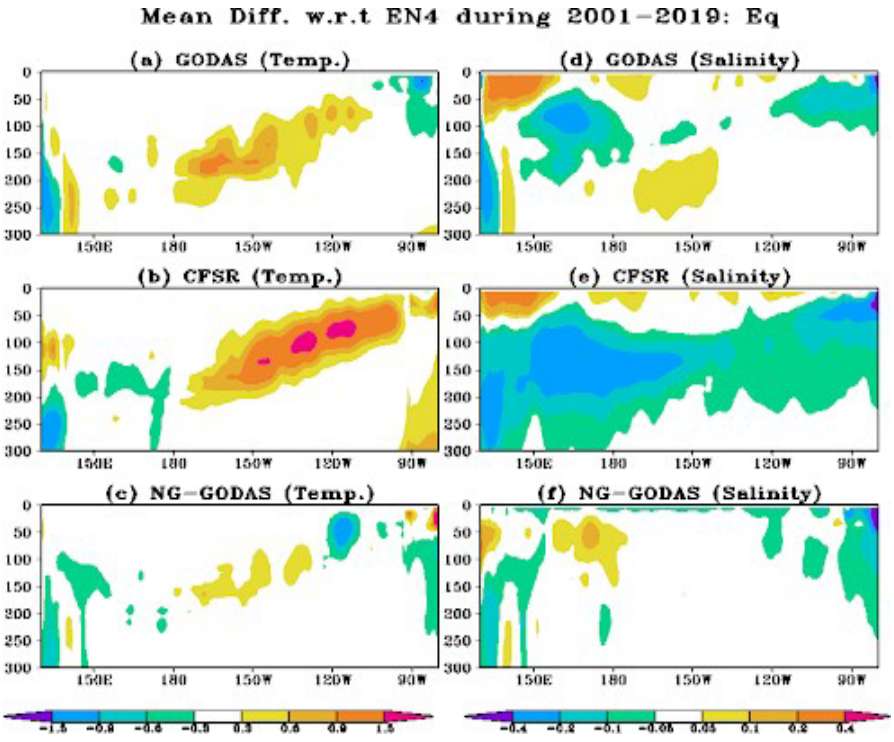

Fig. 14. Mean difference of (a-c) temperature (unit: °C) and (d-f) salinity (unit: psu) along the equator during 2001-2019 with respect to the EN4 analysis in (a, d) GODAS, (b, e) CFSR, and (c, f) NG-GODAS.

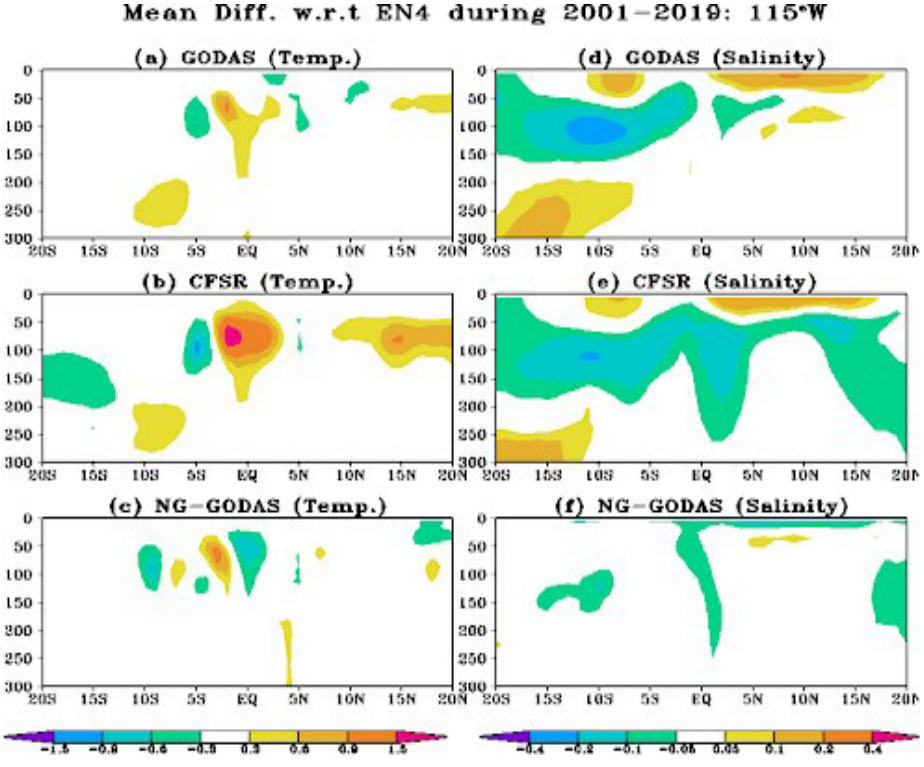

Fig. 15. Mean difference of a)-c) temperature (unit: °C) and d)-f) salinity (unit: psu) along 115oW during 2001-2019 with respect to the EN4 analysis in a), d) GODAS, b), e) CFSR, and c), f) NG-GODAS.

Figures 16 ~ 19 show the root-mean-squared (RMS) differences of temperature and salinity relative to the EN4 analysis for the upper (0-300m) ocean, middle-depth (300-700m) ocean, and the zonal-vertical and meridional-vertical sections. As expected from the salinity assimilation procedure in GODAS and CFSR, NG-GODAS presents a smaller RMS difference in salinity. For temperature, NG-GODAS also demonstrates a smaller RMS difference than CFSR and GODAS.

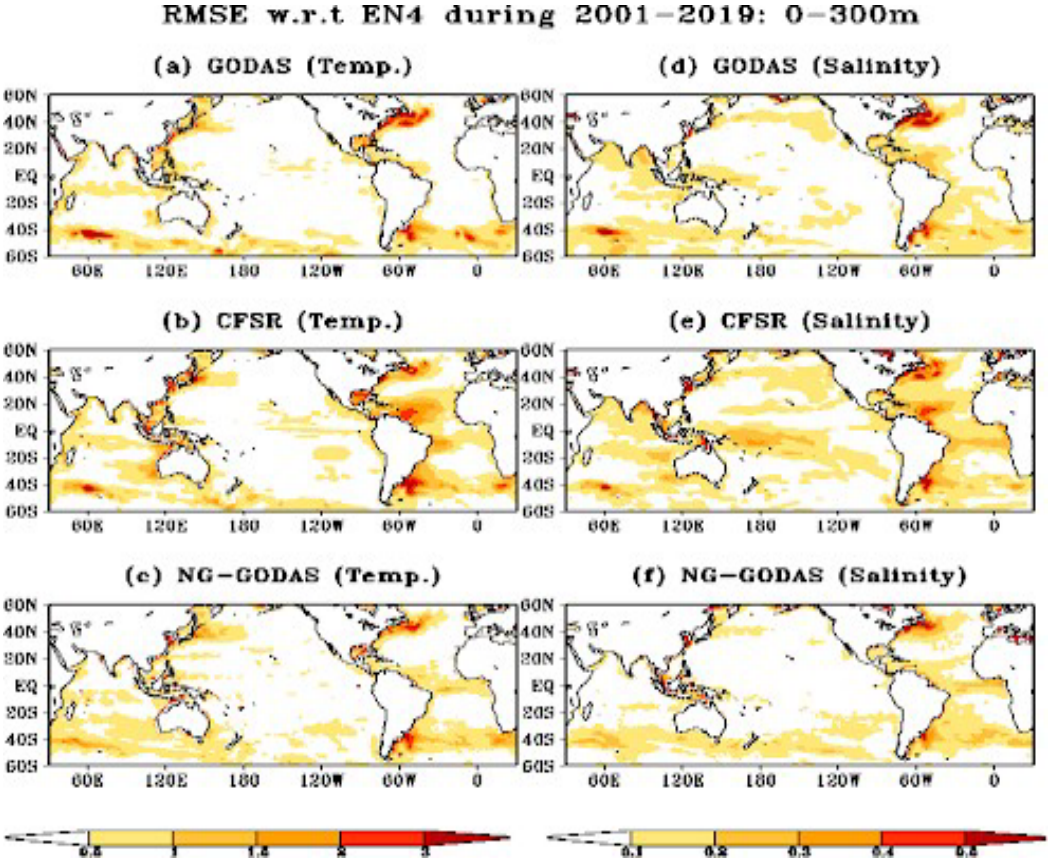

Fig. 16. As in Fig. 12, but for root-mean-squared difference relative to the EN4 analysis.

One exception is over the equatorial Atlantic where GODAS is slightly better than NG-GODAS: compare Figures 16a and 17a to Figs 16c and 17c. A previous diagnostic [Fig. 1 in Zhu et al. (2012b)] suggested that current ocean analysis systems tend to contain much larger uncertainties (noise) in estimating the subsurface oceanic state in the tropical Atlantic compared to the other two tropical oceans, and they are even larger than in the Northern Hemisphere extratropical oceans in the Northern Hemisphere. Zhu et al. (2012a) also found that GODAS is among the best in representing the tropical Atlantic Ocean state. It is noted that one uniqueness of GODAS [Behringer and Xue (2004)] is its application of the incremental analysis update (IAU) scheme, i.e., the analysis increments were gradually incorporated into the model at each time step within an assimilation cycle. In NG-GODAS, by contrast, the analysis increments were inserted into the model only once within an assimilation cycle. The procedure could bring strong shocks in the model at each assimilation cycle, which could result in artificial variations in the ocean. Thus, the application of IAU might be a reason for the better performance of GODAS than NG-GODAS in the equatorial Atlantic where the noise level is high. Overall, the above validations against the EN4 suggest that NG-GODAS present a significant advance over the current NOAA operational ocean analyses – GODAS and CFSR. Currently, we are testing the IAU scheme in NG-GODAS, which we hope will improve its performance in the equatorial Atlantic.

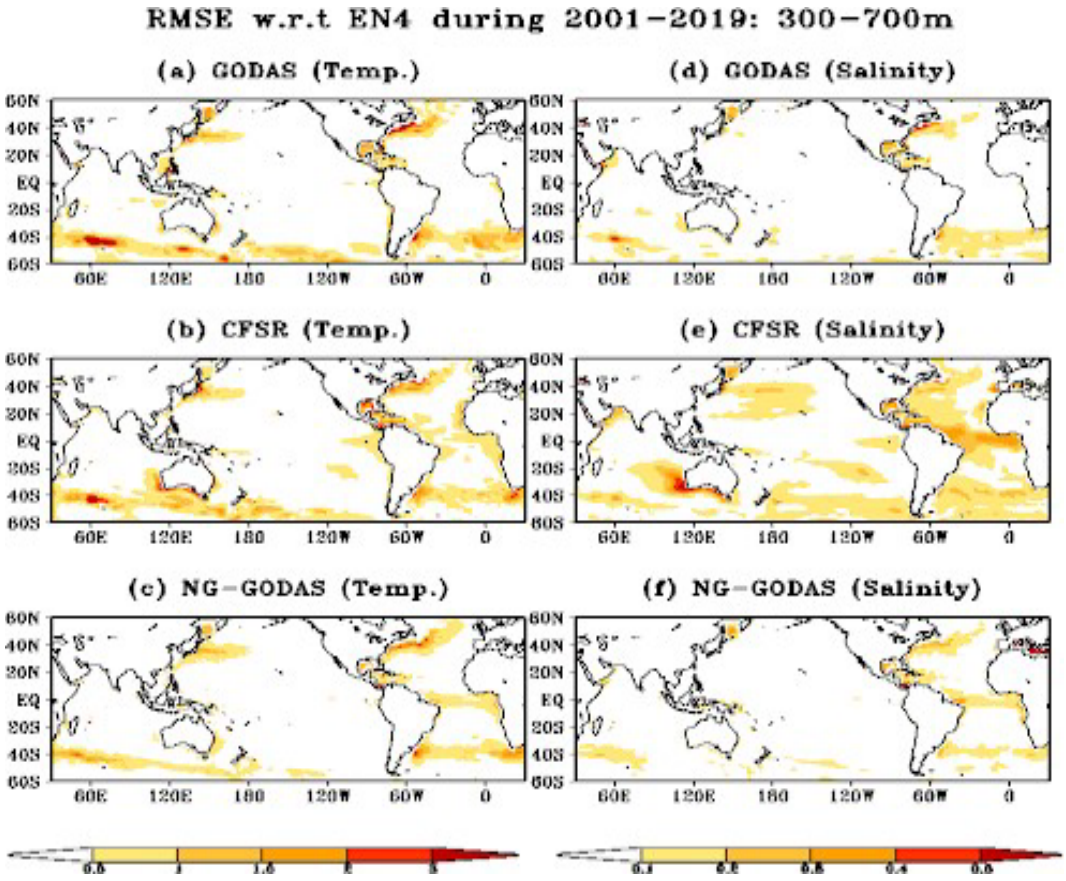

Fig. 17. As in Fig. 13, but for root-mean-squared difference relative to the EN4 analysis.

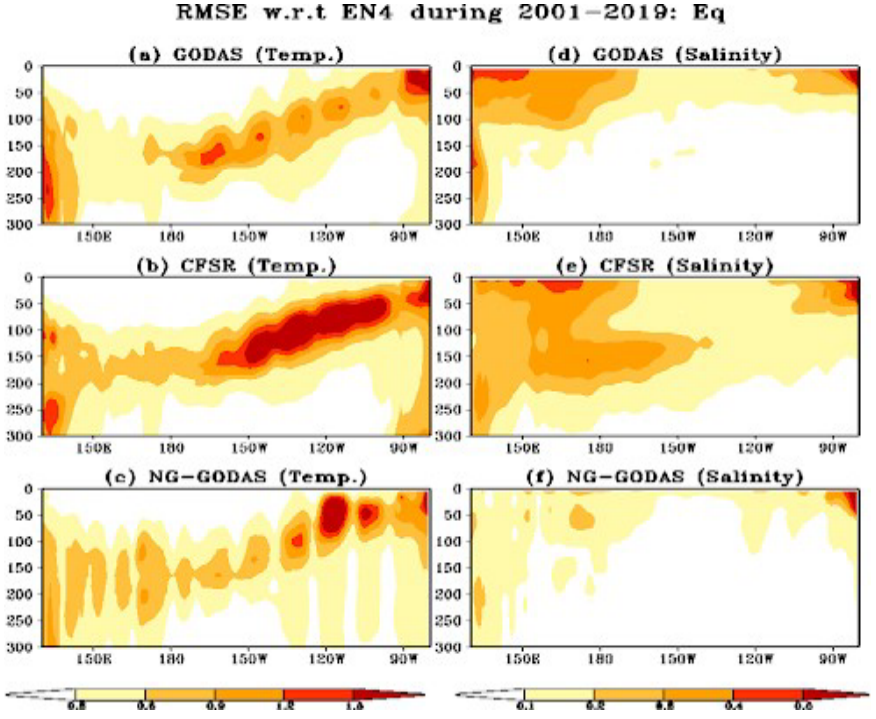

Fig. 18. As in Fig. 12, but for root-mean-squared difference relative to the EN4 analysis.

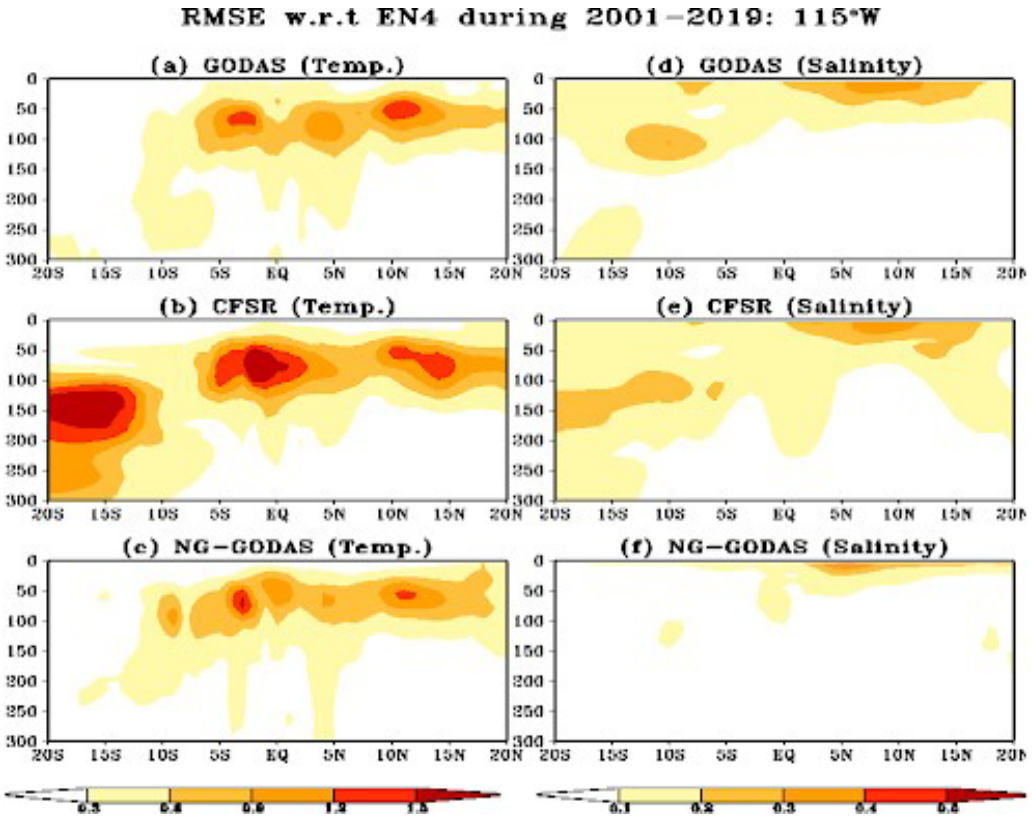

Fig. 19. As in Fig. 13, but for root-mean-squared difference relative to the EN4 analysis.

We also evaluated the Atlantic Meridional Overturning Circulation (AMOC) at 26.5N and compared it with observational estimates from the Rapid Climate Change programme (RAPID). In order to make the most appropriate comparisons to RAPID observations, we calculated NG-GODAS AMOC transports using an analogous "RAPID-style" methodology proposed in Roberts et al. (2013). Velocities in the Florida Straits and the "western boundary wedge" (WBW) are specified to be the same as model velocities. In the RAPID array, the WBW is the region west of 76.75W. In the NG-GODAS setup, the WBW is defined as the region west of 76.50W. The model region is expanded by an additional one grid-point to ensure that the simulated western boundary current is contained within the model WBW. The Ekman transport is derived from the modeled wind stress. The Upper mid-ocean transport (UMO) is split into two components, a sum of mid-ocean geostrophic transport (from 75.50W eastward to 10.50W), and a WBW transport. Finally, a mass-compensation term is applied as a uniform velocity added to the geostrophic velocity field that ensures zero net-flow across the section. The AMOC transport is stronger in the NG-GODAS 3DVar run with a maximum volume transport of 16 Sv at 26.5N, compared with the NG-GODAS-free-run simulation that has a maximum volume transport of 11.3 Sv at 26.5N (Figure 20). The directly measured maximum AMOC transport at 26°N from the RAPID data is about 16.7 Sv for the 2005–2017 period. The simulated AMOC penetration depth from the NG-GODAS 3DVar run is deeper than from the NG-GODAS-free-run, and is close to the observational estimate at 26.5N from the RAPID array (Figure 20).

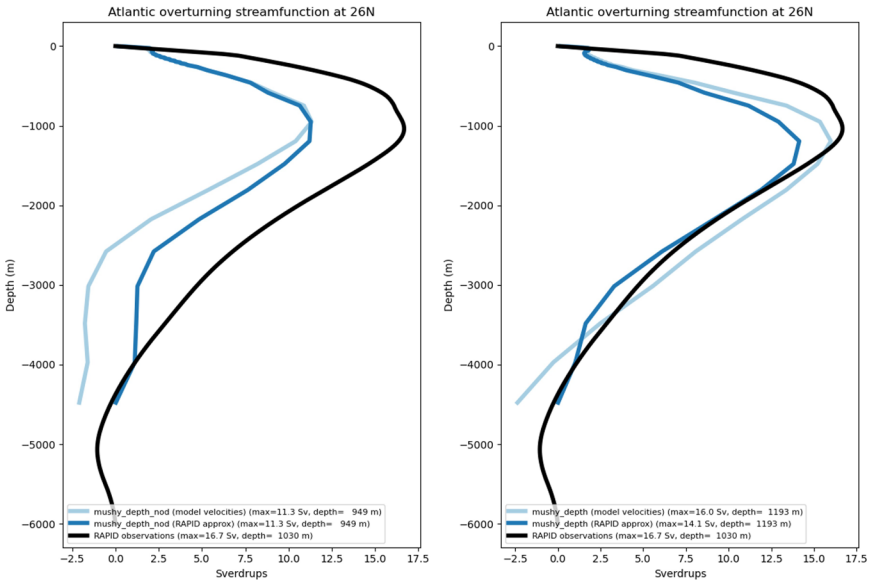

Fig. 20. Time mean (2005-2017) Atlantic meridional overturning stream functions at 26.5°N from RAPID (black), from NG-GODAS modeled velocity field (light blue), and from RAPID-style calculation (dark blue); Left: NG-GODAS-free-run (noda run), Right: NG-GODAS (3dvar run)

The 3DVar sea ice concentration reanalysis result generally provides a better representation of the sea ice extent when compared to the model free run. In Figure 21 and 22, the seasonal sea ice concentration fields computed from the 3DVar analysis and model free runs are compared against the Near-Real-Time NOAA/NSIDC Climate Data Record of Passive Microwave Sea Ice Concentration (https://nsidc.org/data/g10016/versions/2) data set for the 2018-2019 time period. For both marginal and packed sea ice zones, the experiment result demonstrates the 3DVar analysis's ability to constrain the seasonal sea ice anomalies observed in the model free run. Also, the figures show that the data assimilation contribution in the Arctic and Antarctic areas is significantly affected by the sea ice thermodynamics and dynamics conditions including ocean and air interactions and surrounding geographical features. In the Arctic, sea ice extent is limited by the surrounding continents. However, the Antarctic has opposite land-ocean geography where the sea ice forms at latitudes further from the South Pole and expands freely into the surrounding ocean. While the Arctic sea ice concentration consistently improves with the data assimilation, only moderate improvement is observed in the Antarctic area. Sea ice thickness has a direct impact on the atmosphere-ocean heat transfer. The computational results of the total sea ice volumes are compared in Figure 23. Although only sea ice concentration data sets are assimilated in the experiment, 3DVar analysis results provide improved sea ice volume at the Arctic when the results are compared to the model free run and the GIOMAS data. However, it is noted that the NG-GODAS seasonal maximum sea ice volume is significantly lower than the one calculated from the GIOMAS data. For the Arctic, most of the volume reduction for NG-GODAS occurs around 1980, and beyond that there is no clear trend. In the Antarctic, a decades-long overall sea ice increase in the Antarctic area reversed in 2014 and the sea ice extent began to decline from 2014 and stayed at a record low in 2017-2019 time period. Both 3DVar reanalysis and model free results capture a reversed short-term sea ice volume trend that the GIOMAS data set reveals during the 2014-2017 time period. However, marginal contribution of the sea ice concentration data assimilation to the sea ice volume change is found in the Antarctic as well. However, its statistical significance still requires further investigation.

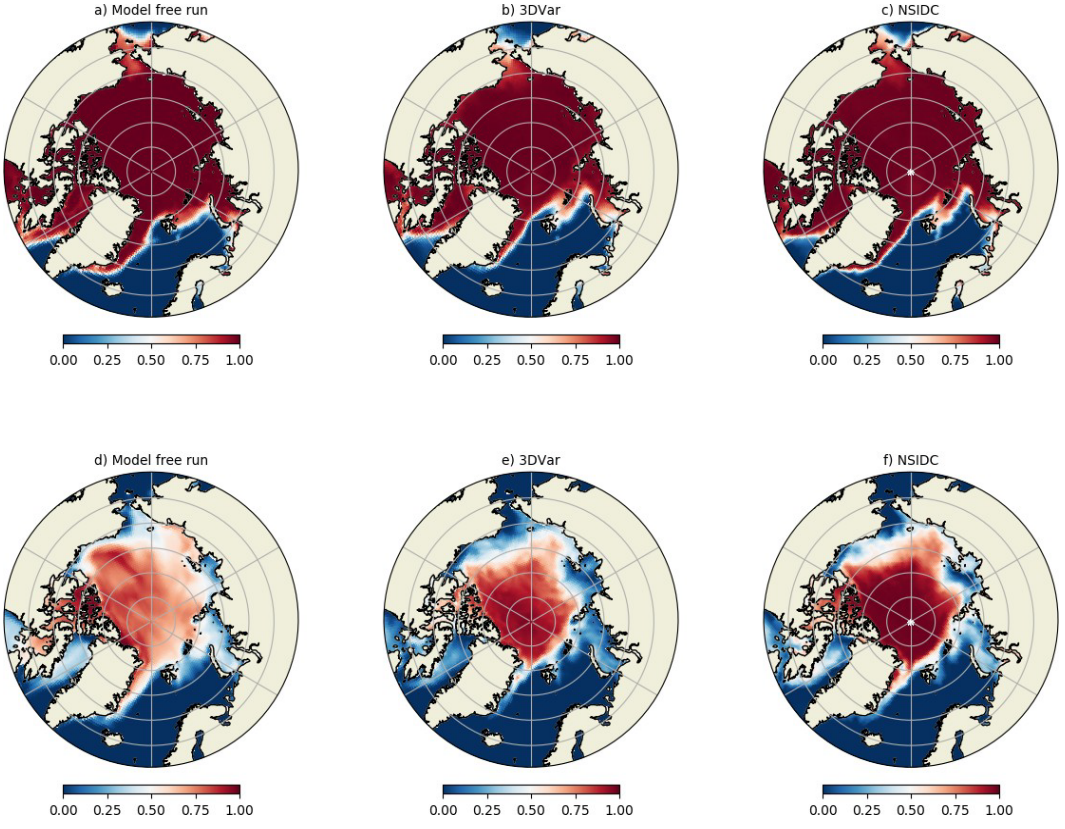

Fig. 21. Arctic seasonal mean sea ice concentration, computed for the 2018-2019 time period: a) model free run DJF (December-January-February), b) 3DVar DJF, c) NSIDC DJF, d) model free JJA (Jun-July-August), e) 3DVar JJA, and f) NSIDC JJA.

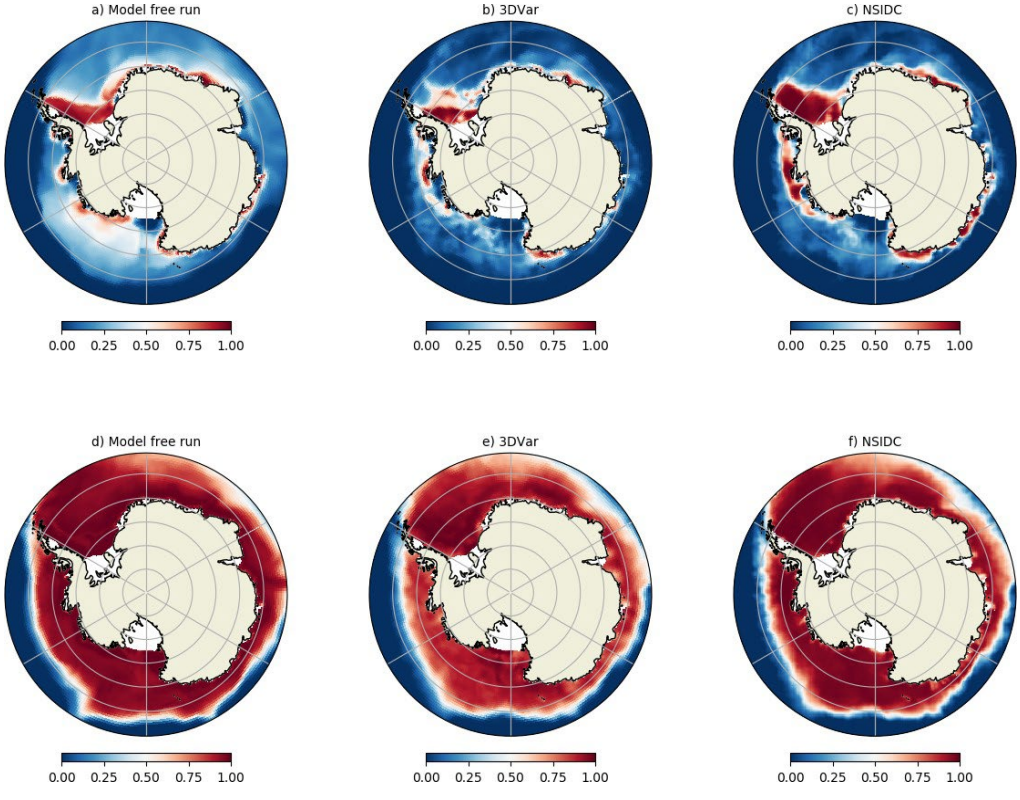

Fig. 22. Antarctic seasonal mean sea ice concentration, computed for the 2018-2019 time period: a) model

free run DJF (December-January-February), b) 3DVar DJF, c) NSIDC DJF, d) model free JJA (Jun-July-August) e) 3DVar JJA, and f) NSIDC JJA.

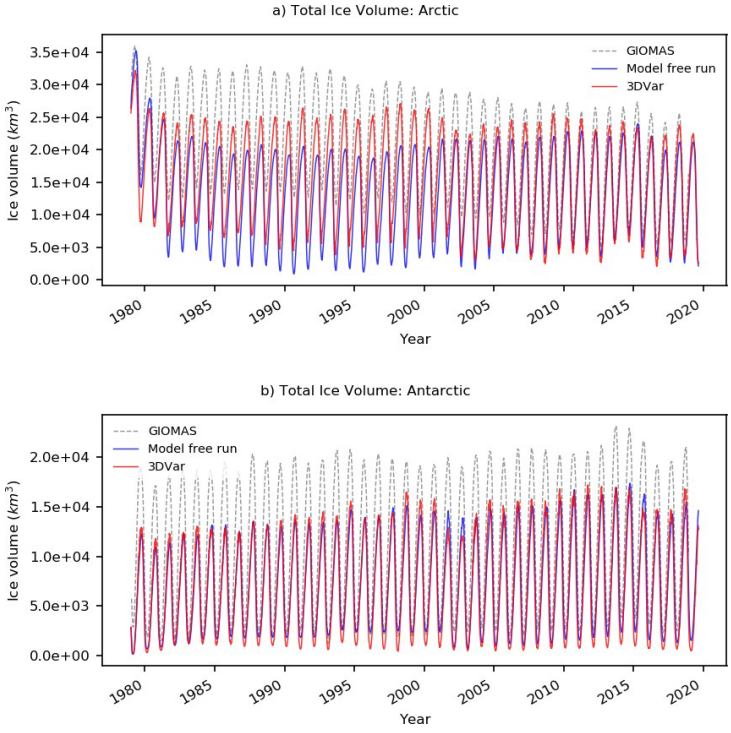

Fig. 23. Comparison of total hemispheric sea ice volume computed from model free run, 3DVar, and GIOMAS data sets.

7. Summary

The NG-GODAS prototype reanalysis experiment from 1979 to 2019 was conducted for the assimilation of extensive marine observation data sets, including in-situ temperature and salinity, sea ice concentration, satellite SST and SSS retrievals, and ADT data sets. The coupled sea ice - ocean reanalysis results were compared with the current operational analysis systems and validated against EN4 and NSIDC data sets. Tuning requirements of the UFS CICE6 model configuration were identified to address sea ice mass balance and stability issues along Antarctic coastal grid points. A climatology sea ice thickness constraint was applied to address divergence in the CICE6 sea ice thickness calculation. The UFS modeling component version updates and modernized JEDI data assimilation system contributed to the improved ocean analysis performance of the NG-GODAS reanalysis run. This result sets the JEDI-based data assimilation system as a building block for the marine component of the future NOAA UFS weakly coupled DA system (GFSv17). Conjointly with the on-going effort to apply the NG-GODAS system to support the UFS S2S initialization project, UFS community feedback will further accelerate the R2O process toward the development of the next generation operational numerical weather prediction system at the National Weather Service (NWS). Key technical conclusions are summarized as follows:

- The NG-GODAS reanalysis results are compared with the current NOAA ocean analysis systems, CFSR and GODAS, and validated against the EN4 product. For both temperature and salinity fields, mean biases and RMSE differences are improved at global scales, but slightly increase over the equatorial Atlantic. Further improvement is anticipated with additional options, such as the IAU capability.
- Large-scale ocean circulation and transport patterns are improved with the 3DVar initialization.

Compared with the model free-run, the reanalysis results show an improved AMOC transport calculation, close to RAPID observations. The simulated NG-GODAS AMOC penetration depth is deeper than the model free-run result and closer to the observational estimate obtained from the RAPID array at 26.5°N.

- The NG-GODAS sea ice - ocean coupled assimilation capability demonstrates improved sea ice predictions in the Arctic. However, only a moderate improvement is found in the Antarctic.
- Sea ice volume calculation results closely follow the GIOMAS product, especially in the Arctic. However, both model free-run and 3DVar analysis results show that considerably lower total ice volumes are obtained by the NG-GODAS.
- The observation-minus-model statistics of the SST and in-situ temperature data sets show model cold bias near the surface layers and warm bias at sub-surface layers. At high latitudes, seasonally varying warm bias is observed in ocean surface layers.
- Satellite SSS OmB and OmA statistics are compared with in-situ salinity assimilation results. Seasonally-varying systematic errors and negative bias are observed in the SMOS SSS statistics. However, such problems are largely contained with the SMAP and Argo salinity data sets.
- Global mean absolute OmB errors of the SSMR, SSMI, and SSMIS sea ice concentration data sets increase during the melting season. Additional observation filter options are needed to enhance the robustness of the sea ice assimilation results in marginal sea ice areas.

Acknowledgments. The UFS data assimilation and reanalysis and re-forecast products produced from the UFS-R2O project are sponsored by the NWS Office of Science and Technology Integration (OSTI) Modeling Program Division and the NOAA's Oceanic and Atmospheric Research (OAR) Weather Program Office (WPO). The project to implement ocean biogeochemical modeling and ocean color data assimilation in NG-GODAS is funded by the JPSS Proving Ground and Risk Reduction (PGRR) Oceans and Coasts Initiative program. Authors thank to Mary Hart at the IMSG/NOAA-NWS-NCEP-EMC for proofreading and editing the article.

APPENDIX A

JEDI SOCA input yaml files

SOCA 3DVar configuration

soca_3dvar.yaml

```
# the list of background files depends on whether we're using ice
_ :       &bkg_files_ocn  ocn_filename : MOM.res.nc
_ :     &bkg_files_ocn_ice
          ice_filename :      cice.res.nc
       << :  *bkg_files_ocn
_ :  &bkg_files *bkg_files___DOMAINS__
# placeholders used by the obs yaml files that will be placed
# where _OBSERVATIONS_ token is
_ :  &obs_distribution RoundRobin
_ :  &obs_error diagonal
_ :  &obs_land_mask
     filter:  Domain  Check
     where:
   - variable:  {name: sea_area_fraction@GeoVaLs}
       minvalue: 0.9
_ :  &observations
       __OBSERVATIONS__
_ :  &soca_vars   __DA_VARIABLES__
variational:
   minimizer:
        algorithm:  RPCG
        iterations:
   - geometry:
           mom6_input_nml: mom_input.nml
        linear model:
           variable change: Identity
            name:  IdTLM
           tstep:  PT1H
            lm  variables:  *soca_vars
            ninner:  150
        gradient  norm reduction:  1e-3
         test:  on
        diagnostics :
          departures:  ombg
        online diagnostics:
         write increment: true
        increment:
```

```
        datadir: Data
        date: &bkg_date __DA_ANA_DATE__
        exp: var.iter1
        type: incr
  output:
    datadir: Data
    exp: 3dvar
    type: an
final:
    diagnostics:
      departures: oman
cost function:
    cost type: 3D-Var
    window begin: __DA_WINDOW_START__
    window length: __DA_WINDOW_LENGTH__
    analysis variables: *soca_vars
    geometry:
      mom6_input_nml: mom_input.nml
    variable change: Ana2Model #Identity
    rotate:
      u: [uocn]
      v: [vocn]
    background:
      read_from_file: 1
      basename: ./bkg/
      date: &bkg_date __DA_ANA_DATE_
      << : *bkg_files
      state variables: *soca_vars
    background error:
      verbosity: main
      covariance model: SocaError
      datadir: ./bump
      strategy: specific_univariate
      load_nicas: 1
      mpicom: 2
      date: *bkg_date
      analysis variables: *soca_vars
      variable changes:
      - variable change: VertConvSOCA
        Lz_min: 0.0
        Lz_mld: 0
        Lz_mld_max: 1.0
```

```
      scale_layer_thick: 5
      input variables: *soca_vars
      output variables: *soca_vars
    - variablechange: BkgErrFILT
      ocean_depth_min: 0 #  [m]
      rescale_bkgerr: 1.0
      efold_z: 2500.0 #  [m]
      input variables: *soca_vars
      output variables: *soca_vars
    - variable change: BkgErrGODAS
      t_min: 0.1
      t_max: 2.0
      t_dz: 20.0
      t_efold: 500.0
      s_min: 0.0
      s_max: 0.25
      ssh_min: 0.0 # value at EQ
      ssh_max: 0.0 # value in Extratropics
      ssh_phi_ex: 20 # lat of transition from extratropics
      cicen_min: 0.1
      cicen_max: 0.1
      hicen_min: 0.1
      hicen_max: 0.1
      input variables: *soca_vars
      output variables: *soca_vars
    - variable change: HorizFiltSOCA
      niter: 2
      filter variables: *soca_vars
      input variables: *soca_vars
      output variables: *soca_vars
    - variable change: BalanceSOCA
      dsdtmax: 0.1
      dsdzmin: 3.0e-6
      dtdzmin: 1.0e-6
      nlayers: 10
      input variables: *soca_vars
      output variables: *soca_vars
observations: *observations
```

APPENDIX B

Implementation of ocean biogeochemical modeling and ocean color data assimilation in the NG-GODAS reanalysis

B1. Introduction

Ocean biogeochemical and ecological forecasts provide early warning of ecosystem changes and their impacts on water quality, human health, and/or regional economies, allowing for sufficient lead time to develop mitigation strategies and take corrective actions. Ocean biogeochemical and ecological processes also provide important geophysical feedback to weather and climate systems, through complex ocean biophysical and ocean-atmosphere interactions. The inability to represent ocean biogeochemical and ecological processes and their feedback to oceanic and atmospheric physics in the current generation of operational forecast systems, as well as our limited understanding of the underlying mechanisms of past extreme weather and ecological events, reduces our capability to predict critical weather conditions and ecological "tipping points" and affects management effectiveness at both global and regional scales. Through a project funded by the JPSS Proving Ground and Risk Reduction (PGRR) program, we developed and evaluated ocean biogeochemical modeling and ocean color data assimilation tools as well as the required infrastructure within the NG-GODAS in support of NOAA/NCEP's operational weather, S2S, and ecological predictions. This appendix provides an overview of key milestones of the implementation of the BLING-based ocean biogeochemistry assimilation capability for the application of the satellite-based ocean color observations in the NG-GODAS framework. The released ocean biogeochemical reanalysis file set is the 2003-2013 UFS-DATM-MOM6-BLINGv2-CICE6 (at a horizontal resolution of 1°) ocean reanalysis 24-hour cycle output. Analyzed ocean biogeochemical variables include chlorophyll (Chl-a), particulate organic phosphate (POP), and dissolved inorganic phosphate (DIP) concentrations. This file set is in contrast to the 2003-2013 ocean physics only, UFS-DATM-MOM6-CICE6 ocean reanalysis output. Both reanalysis experiments used identical model configurations and physical ocean observational data sets except that the first file set had the BLING model and ocean color data assimilation options enabled. Both file sets are publicly available at https://registry.opendata.aws/noaa-ufs-marinereanalysis.

B2. Ocean biogeochemical model

Coupled to the MOM6 model component to the UFS system, the biogeochemistry model is adapted from NOAA/GFDL's BLING model (Biogeochemistry with Light, Iron, Nutrients and Gas version 2, or BLINGv2). BLINGv2 states are essentially treated as generic tracers in MOM6, and so are subject to advective and diffusive transports, as well as source and sink terms from boundary fluxes (e.g., atmospheric deposition, riverine inputs) and biogeochemical processes (e.g., burial, denitrification). The coupled MOM6-BLINGv2 model has been successfully tested at horizontal resolutions of 1° and 0.25° using NG-GODAS. Preliminary results suggest that upper-ocean physics (e.g., SST) are moderately sensitive to ocean biogeochemical (e.g., Chl-a) variability with a response of up to 1°C in some regions (Figure B1).

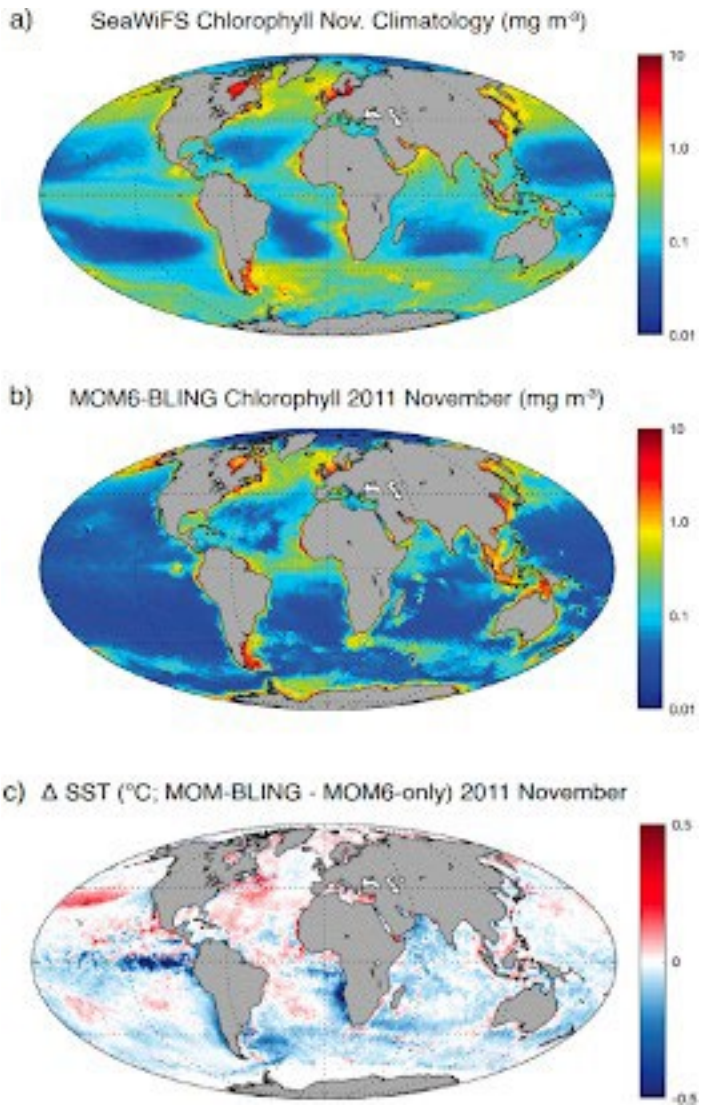

Fig. B1. a) SeaWiFS Chl-a climatology (Nov.) used to calculate short-wave radiation penetration in the MOM6 physics-only run; b) MOM6-BLING simulated Chl-a averaged over November 2011; and c) difference in sea surface temperature (SST) between the two experiments, suggesting that upper-ocean physics, such as SST, are sensitive to Chl-a variability.

B3. Ocean color data assimilation

As mentioned in the main text, NG-GODAS employs JEDI-SOCA interface. The JEDI project is the backbone for performing data assimilation across the variety of the UFS model applications. We further developed the SOCA interface to allow the integration of near-real-time satellite ocean color products into MOM6-BLINGv2 simulations.

Ocean color observations

Level-2 data streams have been established from NESDIS into NCEP for NOAA-20/VIIRS and S-NPP/VIIRS historical and near-real-time ocean color observations (i.e., chlorophyll concentration, or Chl-a, and particulate organic carbon, or POC), specifically from NOAA CoastWatch and NASA OB.DAAC to NOAA's Research and Development High-Performance Computing System (RDHPCS). The required software to preprocess VIIRS Level-2 ocean color products for basic quality control and ingestion by the JEDI system were developed. Specifically, these observations

are converted into a unified data format (i.e., IODA compatible) that can be ingested by any model employing the JEDI system for data assimilation.

Chl-a and POC analysis

To assimilate Chl-a and POC, the corresponding biogeochemical states saved in the model restart file are updated during each data assimilation cycle (i.e., 24h) based on increments calculated in JEDI/SOCA. Other key states, such as dissolved inorganic phosphate (DIP) concentration, are updated by solving BLING internal equations for phytoplankton growth and nutrient limitation based on Chl-a or POC increments. The diagonal background error covariance ("B") matrix for the ocean color observations is computed using the SABER-BUMP package of JEDI. For each grid-point, the observational error variance will be set to be proportional to the observed values [e.g., observational error = 30 for Chl-a; Tsiaras et al. (2017)]. The JEDI-UFO estimates "ocean color" properties from the biogeochemical model as the corresponding variables averaged over the first optical depth at each grid-point. Figure B2 shows a preliminary Chl-a daily analysis using the JEDI-SOCA 3DVAR scheme. We also performed preliminary evaluation of a long-term (10-year, 2003-2012) Chl-a analysis using the mentioned 1° ocean physical-biogeochemical analysis experiment setup. Figure B3 shows the relative model and analysis bias calculated as the model-observational difference divided by observed value at the corresponding location plus a small scaling coefficient (0.001). In the experiment, Level-3 Aqua/MODIS Chl-a observations were assimilated in the BLING biogeochemical model. The results suggested that daily assimilation of ocean color observations reduced the mean relative model Chl-a bias for 24-hr model forecasts from approximately 55% to 30% on a global scale.

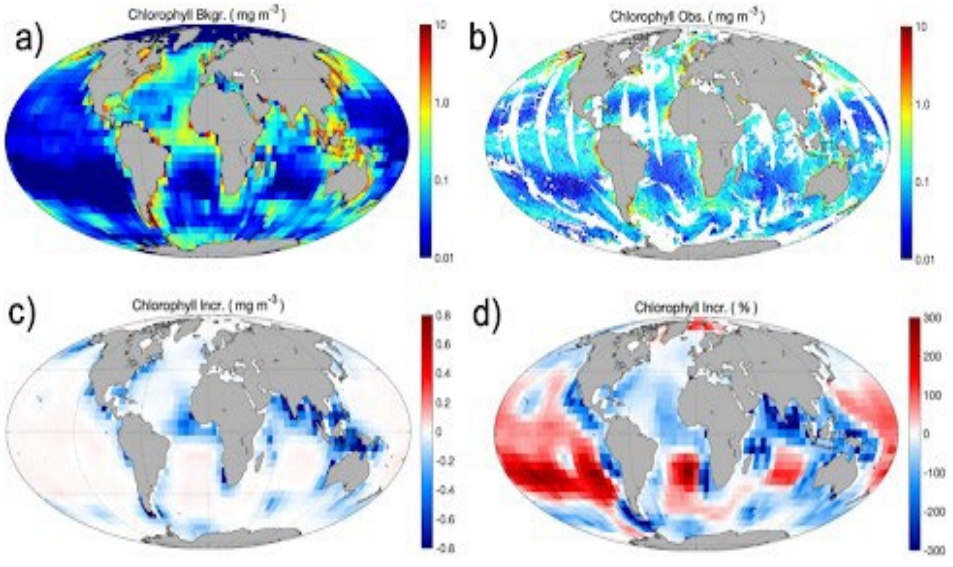

Fig. B2. a) MOM6-BLING simulated "background" Chl-a on 2018/04/15, b) Level-2 Chl-a derived from NOAA-20/VIIRS imagery on 2018/04/15, which was used for Chl-a assimilation, c) and d) Chl-a increments calculated based on the 3DVAR scheme in JEDI/SOCA, shown as absolute increment (c) and percentage change compared to "background" (d), respectively.

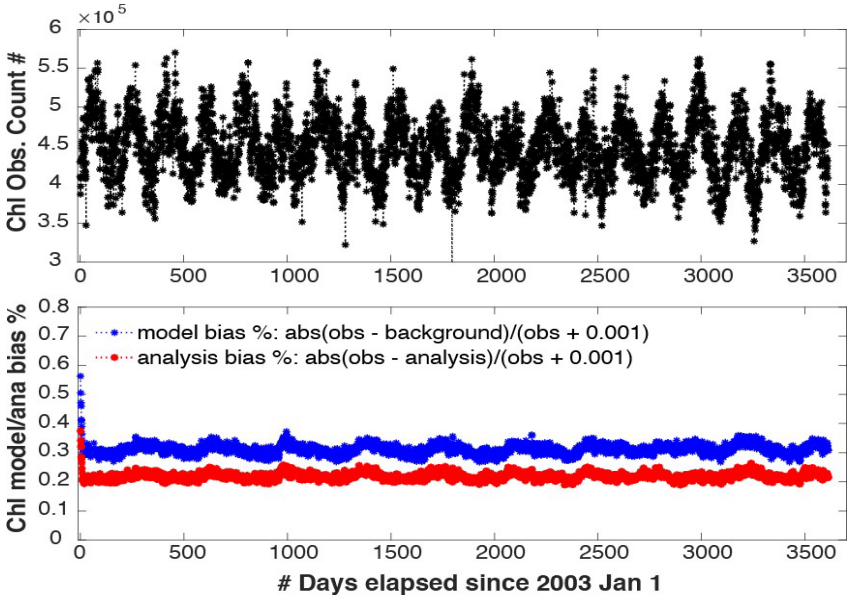

Fig. B3. Coupled ocean physical-biogeochemical analysis experiment results: daily assimilated Level-3 Aqua/MODIS Chl-a observation count on the top panel. Y-axis on the bottom panel shows global mean absolute relative model and analysis biases calculated as model-minus-observation divided by observation with scaling coefficient (0.001) added.

References

Adcroft, A., and Coauthors, 2019: The GFDL global ocean and sea ice model om4. 0: Model description and simulation features. *Journal of Advances in Modeling Earth Systems*, **11-10**, 3167–3211.

Behringer, D. W., and Y. Xue, 2004: Evaluation of the global ocean data assimilation system at ncep: The Pacific Ocean Eighth Symposium on Integrated Observing and Assimilation Systems for Atmosphere, Oceans, and Land Ssurface. *AMS 84th Annual Meeting, Washington State Convention and Trade Center, Seattle, Washington, 11-15*.

Bitz, C., and W. H. Ipscomb, 1999: An energy-conserving thermodynamic model of sea ice. *Journal of Geophysical Research Atmospheres*, **1041**, 15 669–15 678.

Boyer, T., and Coauthors, 2018: World Ocean Database 2018. A.V. Mishonov, Technical Ed., NOAA Atlas NESDIS 87. https://www.ncei.noaa.gov/sites/default/files/2020-04/wod_intro_0._pdf

Cavalieri, D. J., C. L. Parkinson, P. Gloersen, and H. J. Zwally., 1996: Sea ice concentrations from nimbus-7 smmr and dmsp ssm/i-ssmis passive microwave data, version 1. NASA National Snow and Ice Data Center Distributed Active Archive Center, doi: https: //doi.org/10.5067/8GQ8LZQVL0VL.

Cooper, M., and K. Haines, 1996: Altimetric assimilation with water property conservation. *Journal of geophysical research*, **101-C1**, 1059–1077.

Derber, J. C., and A. Rosati, 1989: A global oceanic data assimilation system. *J. Phys. Oceanogr.*

Dunne, J. P. D., and Coauthors, 2020: Simple global ocean biogeochemistry with light, iron, nutrients and gas version 2 (blingv2): Model description and simulation characteristics in gfdl's cm4.0. *Journal of Advances in Modeling Earth Systems*, **12-10**, doi: 10.1029/2019MS002 008.

Dussin, R., B. Barnier, L. Brodeau, and J. M. Molines, 2016: The making of the drakkar forcing set dfs5. Tech. Rep. 1–34, DRAKKAR/MyOcean, The address of the publisher. Report 01-04-16.

Embury, O., C. Bulgin, and J. Mittaz, 2019a: Along-track scanning radiometer (atsr) level 2 preprocessed (l2p) climate data record version 2.1 centre for environmental data analysis. https://doi.org/10.5285/916b93aaf1474ce793171a33ca4c5026.

Embury, O., C. Bulgin, and J. Mittaz, 2019b: Temperature climate change initiative (sst cci): Advanced very high resolution radiometer (avhrr) level 2 preprocessed (l2p) climate data record version2.1 centre for environmental data analysis. https://doi.org/10.5285/373638ed9c434e78b521cbe01ace5ef7.

Feltham, D. L., N. Untersteiner, J. S. Wettlaufer, and M. Worster, 2006: Sea ice is a mushy layer. *Geophys. Res. Lett.*, **33**.

Ganachaud, A., and C. Wunsch, 2003: Large-scale ocean heat and freshwater transports during the world ocean circulation experiment. *Journal of Climate*, **16 (4)**, 696 – 705, doi: 10.1175/1520-0442(2003)016<0696:LSOHAF>2.0.CO;2, URL https://journals.ametsoc.org/view/journals/clim/16/4/1520-0442_2003_016_0696_lsohaf_2.0.co_2.xml.

Good, S. A., M. J. Martin, and N. A. Rayner, 2013a: En4: quality controlled ocean temperature and salinity profiles and monthly objective analyses with uncertainty estimates. *Journal of Geophysical Research: Oceans*, **118**, 6704–6716.

Good, S. A., M. J. Martin, and N. A. Rayner, 2013b: En4: Quality controlled ocean temperature and salinity profiles and monthly objective analyses with uncertainty estimates. *Journal of Geophysical Research*, **118**, 6704–6716.

Holdaway, D., G. Vernières, M. Wlasak, and S. King, 2020: Status of model interfacing in the joint effort for data assimilation integration (jedi). *JCSDA Quarterly*, **66**.

Honeyager, R., S. Herbener, X. Zhang, A. Shlyaeva, and Y. Trémolet, 2020: Observations in the joint effort for data assimilation integration (jedi) - ufo and ioda. *JCSDA Quarterly*, **66**.

Hunke, E., and Coauthors, 2020: CICE-Consortium/Icepack: Icepack 1.2.4 (Version 1.2.4). Zenodo. http://doi.org/10.5281/zenodo.4358418.

Large, G., and S. G. Yeager, 2004: Diurnal to decadal global forcing for ocean and sea-ice models: The data sets and flux climatologies.

Lu, F., and Coauthors, 2020: GFDL's spear seasonal prediction system: initialization and ocean tendency adjustment (ota) for coupled model predictions. *Journal of Advances in Modeling Earth Systems*.

Merchant, C. J., and Coauthors, 2019: Satellite-based time-series of sea-surface temperature since 1981 for climate applications. *Sci. Data*, **6**, 223.

Pryamitsyn, V., A. Ignatov, B. Petrenko, O. Jonasson, and Y. Kihai, 2020: Evaluation of the initial NOAA AVHRR GAC SST reanalysis version 2 (RAN2 B01). *Ocean Sensing and Monitoring XII*, W. W. Hou, and R. A. Arnone, Eds., SPIE, International Society for Optics and Photonics, Vol. 11420, 1 – 16, doi:10.1117/12.2558751, URL https://doi.org/10.1117/12.2558751.

Roberts, C. D., and Coauthors, 2013: Atmosphere drives recent interannual variability of the atlantic meridional overturning circulation at 26.5°n. *Geophysical Research Letters*, **40 (19)**, 5164–5170, doi:https://doi.org/10.1002/grl.50930, URL https://agupubs.onlinelibrary.wiley.com/doi/

abs/10.1002/grl.50930, https://agupubs.onlinelibrary.wiley.com/doi/pdf/10.1002/grl.50930

Saha, S., and Coauthors, 2006: The ncep climate forecast system. *Journal of Climate*, **19**, 3483–3517.

Saha, S., and Coauthors, 2010: The ncep climate forecast system reanalysis. *Bulletin of the American Meteorological Society*, **91-8**, 1015–1058.

Scharroo, R., E. W. Leuliette, J. L. Lillibridge, D. Byrne, M. C. Naeije, and G. T. Mitchum, 2013: Rads: Consistent multi-mission products, in proc. of the symposium on 20 years of progress in radar altimetry. Eur. Space Agency Spec. Publ., ESA SP-710, p. 4 pp., Venice, 20-28 September.

Sluka, T., 2018: Strongly coupled ocean-atmosphere data assimilation with the local ensemble transform kalman filter. Ph.D. thesis, University of Maryland College Park.

Troccoli, A., and Coauthors, 2002: Salinity adjustments in the presence of temperature data assimilation. *Monthly Weather Review*, **130-1**, 89–102.

Trémolet, Y., 2020: Joint effort for data assimilation integration (jedi) design and structure. *JCSDA Quarterly*, **66**.

Tsiaras, K. P., I. Hoteit, S. Kalaroni, G. Petihakis, and G. Triantafyllou, 2017: A hybrid ensemble-oi kalman filter for efficient data assimilation into a 3-d biogeochemical model of the mediterranean. *Journal of Advances in Modeling Earth Systems*, **67-6**, 673– 690.

Weaver, A. T., C. Deltel, E. Machu, S. Ricci, and N. Daget, 2006: A multivariate balance operator for variational ocean data assimilation. *Quarterly Journal of the Royal Meteorological Society*, **131**, 3605–3626.

Zhang, J., and D. Rothrock, 2003: Modeling global sea ice with a thickness and enthalpy distribution model in generalized curvilinear coordinates. *Mon. Wea. Rev.*, **131**, 681–697.

Zhu, J., B. Huang, and M. A. Balmaseda, 2012a: An ensemble estimation of the variability of upper-ocean heat content over the tropical atlantic ocean with multi-ocean reanalysis products. *Clim. Dyn.*, **39**, 1001–1020, doi: 10.1007/s00 382–011–1189–8.

Zhu, J., B. Huang, L. Marx, J. L. K. III, M. A. Balmaseda, R.-H. Zhang, and Z.-Z. Hu, 2012b: Ensemble enso hindcasts initialized from multiple ocean analyses. *Geophysical Research Letters*, **39-9**, L09 602, doi: 10.1029/2012GL051 503, 2012L09 602.